SAFIYAH BT. PIRMANG

B.ENG (HONS) CHEMICAL ENGINEERING

SEPTEMBER 2015

# CONSEQUENCE STUDY OF $CO_2$ LEAKAGE IN SEAWATER USING COMPUTATIONAL FLUID DYNAMIC (CFD) APPROACH

**SAFIYAH BINTI PIRMANG**

CHEMICAL ENGINEERING

UNIVERSITI TEKNOLOGI PETRONAS

SEPTEMBER 2015

# Consequence Study of $CO_2$ Leakage in Seawater using Computational Fluid Dynamic (CFD) Approach

by

Safiyah Binti Pirmang

15628

Dissertation submitted in partial fulfillment of
the requirements for the
Bachelor of Engineering (Hons)
(Chemical Engineering)

SEPTEMBER 2015

Universiti Teknologi PETRONAS,
32610, Bandar Seri Iskandar,
Perak Darul Ridzuan.

CERTIFICATION OF APPROVAL

**Consequence Study of $CO_2$ Leakage in Seawater using Computational Fluid Dynamic (CFD) Approach**

by

Safiyah Binti Pirmang
15628

A project dissertation submitted to the
Chemical Engineering Programme
Universiti Teknologi PETRONAS
in partial fulfillment of the requirement for the
BACHELOR OF ENGINEERING (Hons)
(CHEMICAL ENGINEERING)

Approved by,

_____
(Dr. Risza Bt Rusli)

UNIVERSITI TEKNOLOGI PETRONAS
BANDAR SERI ISKANDAR, PERAK.
SEPTEMBER 2015

CERTIFICATION OF ORIGINALITY

This is to certify that I am responsible for the work submitted in this project, that the original work is my own except as specified in the references and acknowledgements, and that the original work contained herein have not been undertaken or done by unspecified sources or persons.

_____

SAFIYAH BINTI PIRMANG

## ABSTRACT

The climate change due to the effect of greenhouse gas-$CO_2$ is considered a risk to environment as well as humanity. The promising mitigation action to solve this problem is the implementation of Carbon Capture and Storage (CCS) application. However, major concern identified with CCS, is the likelihood of $CO_2$ leakage and their effect to the marine ecosystem and environment. Therefore, the study of this project involves modeling the $CO_2$ leakage from potential seawater storage and to predict the consequences of $CO_2$ leakage in seawater through evaluating the dissolution rate of $CO_2$ bubble. The leakage scenarios are adopted from the recent QICS experiment in the Scottish sea at Ardmucknish Bay. The modeling approach for the study will be based on Computational Fluid Dynamic (CFD) approach with reference from existing mathematical model. ANSYS Fluent software was used for the simulation are to illustrate the bubble characteristic in terms of size distribution, velocity, bubble dissolution and dispersion, transport and chemical reaction (pH change). All of these factors were analyzed to evaluate the impact of $CO_2$ leak to the local marine environment and to validate the mathematical modeling develop by other researcher using an extensive CFD simulation approach.

## ACKNOWLEDGEMENT

First and foremost, I would like to take this opportunity to express my profound gratitude and thank you to my parents for their continuous support and encouragement to complete this Final Year Project (FYP) course.

Special thanks to my supervisor, Dr. Risza Binti Rusli for her continuous monitoring, guidance and advice throughout the course. She has been very supportive and very thoughtful that help me along the way of completing this project. Not to forget to Mr. Loi Pham for his support and effort to assist me in all possible way to solve any difficulties that I faced. My deepest thank to him who always allow me to question and giving prompt reply for my doubt in all fields. My greatest gratitude is also extended to FYP coordinators who provide all materials related to this course and assisting us throughout the whole semester.

Next, I would like to thank to my lecturers, seniors and friends who are very kind in providing information, knowledge and help me in various ways through thick and thin of time. The kindness and continuous support from them has enabled me to complete this project.

Furthermore, deepest thank to Department of Chemical Engineering, Universiti Teknologi PETRONAS for providing platform for us to learn and explore as much as possible by conducting this final year project. Without the facilities provided, this project cannot be accomplished. Lastly, I would like to thank to everyone who directly or indirectly help me in this project.

Thank you.

## TABLE OF CONTENT

**LIST OF FIGURES**

**LIST OF FIGURES**

## LIST OF TABLES

# CHAPTER 1

# INTRODUCTION

## 1.1 Background Study

Carbon dioxide ($CO_2$) gas is found in small proportions in the atmosphere. It is produced from the combustion of coal or hydrocarbon, fermentations of liquids and the breathing of human and animals. $CO_2$ is also found beneath the earth surface and other places where the earth crust is thin. It is found in great depth of sea and commingled with oil and gas deposits. $CO_2$ is a greenhouse gas that is responsible causing the earth to be warmer and give a significant impact to the climate changes which urge the demand of reducing $CO_2$ emission to the atmosphere.

Carbon Capture and Storage (CCS) is one of the approaches to mitigate the climate change by capturing carbon dioxide from large point of sources such as power plants or industrial sources and subsequently storing it in underground safely, instead of releasing to the atmosphere (Han, Ahn, Lee & Lee', 2012). CCS involve the use of technology, first to collect and concentrate the $CO_2$ produced in industrial and energy related sources, transport it to a suitable storage location and store it away from the atmosphere for a long period. FIGURE 1.1 illustrates the CCS system from the source to process; capture; transport and storage.

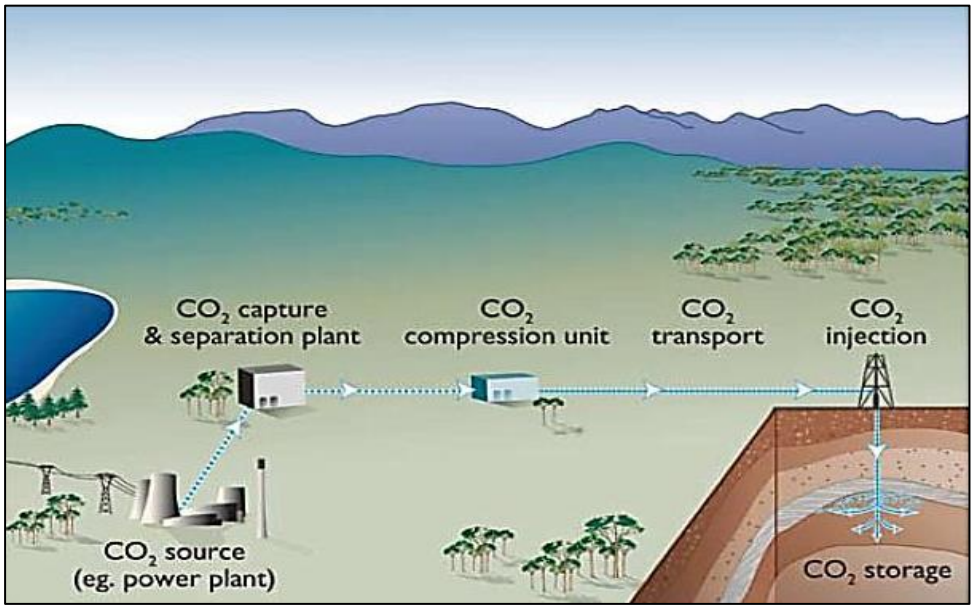


FIGURE 1.1 Example of CCS system (Cooperative Research Centre for Greenhouse Gas Technologies ($CO_2$CRC)).

The carbon capture system are varies according to the technology deployed by different country and industries. Some technologies are extensively used in mature markets especially for oil and gas industry, while others are still in research and development stages.

## 1.2 Problem Statement

$CO_2$ has been recognized as a significant workplace hazard for over 100 years, resulting many standards and legislative control that have been established to maintain an acceptable level of risk for those who could harmed by it (Harper, Wilday & Bilio, 2011). $CO_2$ is present in the atmosphere at a concentration of approximately 385 ppm. With the accelerating process of industrial and manufacturing sector as well as burning of fossil fuels the $CO_2$ concentration in the earth's atmosphere has exceeded 400 ppm by May 2013 (Cai, Bauer, Raymond, Bianchi, Hopkinson & Regnier, 2013). $CO_2$ released into the atmosphere leading to the greenhouse, global warming, rising of sea level and the rest that released into the sea, leading to an ocean acidification (Luo, 2012). $CO_2$ being a potent greenhouse gas lead to the dramatic consequence to the rise for global temperatures and to some extent deteriorated the ocean pH. So as the threat of global warming and acidification

become more real, the political, social and environment pressure to reduce $CO_2$ emissions continue to grow.

CCS in deep or sub-surface geological reservoirs has been proposed as a credible mitigation approach to climate change issue (J. Blackford et al., 2015). Han et al. (2012) stated that, the CCS process evolved in capturing $CO_2$ from the power plants and industrial resources and then injected it into deep sub-seabed reservoir or geological structure for permanent storage (Sellami, Dewar, Stahl, & Chen, 2015). The major concern in execution of the CCS application is the risk and potential impacts of $CO_2$ leakage from the storage that might affect the marine environment (Dewar, Wei, McNeil, & Chen, 2013a). Thus, it is necessary to study the consequence of the leak with regards to the toxicity of $CO_2$ towards the environment especially to the marine life for under seabed storage (Noble et al., 2012). The consequence study conducted in this project will demonstrates the Computational Fluid Dynamic (CFD) approach in predicting the hazard of $CO_2$ released by working on the existing mathematical model and ongoing research.

## 1.3 Objective and Scope of study

### 1.3.1 Objective

The main objectives of this study are;

i) To study the consequence of $CO_2$ leakage through bubble dissolution in seawater.
ii) To evaluate the change in seawater pH due to CO2 bubble dissolution
iii) .To validate existing experimental and mathematical modeling of the dynamic rising of CO2 bubble using a CFD approach

### 1.3.2 Scope of study

The scope of the study will only cover the scenario of $CO_2$ leakage in seawater. Several small-scale experiment related to the $CO_2$ leak in seawater will be used as the reference for model validation. Consequence model by CFD related to

the $CO_2$ release relating to pipeline release of some liquid or gas to the atmosphere are well developed. However, less number of extensive research or experimental study for modeling of subsea releases, so generally there is a high degree of uncertainty in the modeling methodology and conservatism is often used (Bai & Bai, 2014). Meanwhile, studies of impact of $CO_2$ leakage to the marine life are also still in research phase and source of information are limited. But, several study are well developed regarding the transfer of $CO_2$ bubbles into the surrounding water which can be used to predict the potential impact of $CO_2$ release to marine ecosystem (Beaubien et al., 2014). Therefore, this project will mainly focused on the consequences of $CO_2$ leakage in seawater and use a comprehensive CFD tools to model the rising of $CO_2$ bubbles by critically analyze and validating the existing experimental data and mathematical model. The experimental results of Quantifying and Monitoring Potential Ecosystem Impact of Geological Carbon Storage (QICS) project are used for model validation.

# CHAPTER 2

# LITERATURE REVIEW

## 2.1 $CO_2$ Properties

Pure $CO_2$ exhibits triple-point behavior dependent on the temperature and pressure. The triple point is defined as temperature and pressure where three phases (gas, liquid, solid) can exist simultaneously in thermodynamic equilibrium as shown in FIGURE 2.1.

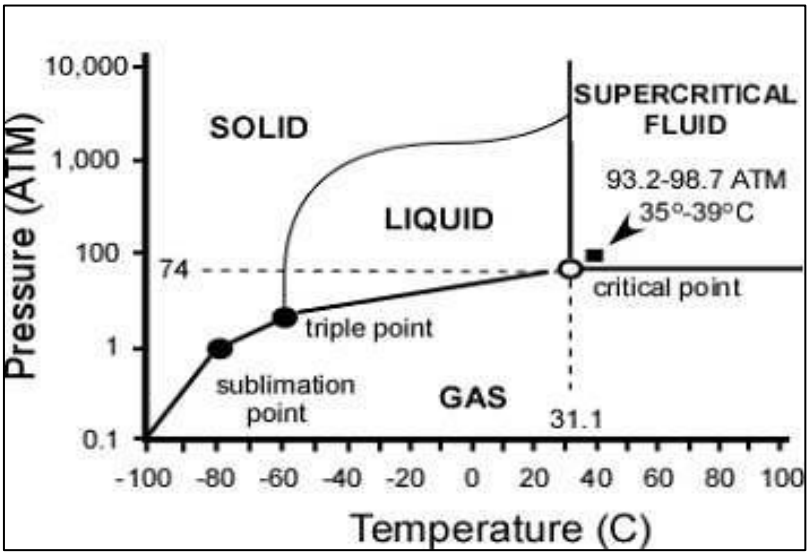


FIGURE 2.1 $CO_2$ Phase Diagram

Above the critical point, the liquid and gas phases cannot exist as separate phase where $CO_2$ develops supercritical properties that have some characteristic of a gas and others of a liquid. In the event of uncontrolled or bulk released of $CO_2$, a portion of the escaping fluid will quickly expand to $CO_2$ gas. In this circumstances, the temperature of the released gas will fall rapidly due to the pressure drop (Joule Thompson Effect) and the phase changes.

According to Global CCS Institute (2013), for above ground application at low temperature some of the released $CO_2$ formed $CO_2$ 'snow' results in cooled down of surrounding air. This happen when the water vapour in the air condense locally and resembles thick fog. In contrast for most subsea application, the $CO_2$ will expand to a gas as a result of expanding into the lower pressure of water. Heat from the water will quickly absorbed and $CO_2$ gas, being less dense than seawater $CO_2$ will tend to rise toward the surface.

## 2.2 Carbon Capture and Storage (CCS)

CCS provides the only solution to transform fossil fuel based power generation and some other industrial processes to relatively low carbon emissions, consistent with climate change mitigation (Phelps et al., 2015). The general idea is that, $CO_2$ is captured from the power plant, industries or any other point of sources, compressed, transported and finally injected in deep underground for permanent storage (Gibbins & Chalmers, 2008). Available technology of CCS could reduce $CO_2$ emission to the atmosphere by approximately 80 to 90 percent (IPCC, 2005). The net reduction of $CO_2$ emissions to the atmosphere through CCS depends on the fraction of $CO_2$ captured.

Carbon Capture and Storage Association (CCSA) claim that, the CCS chain consists of three parts; capturing, transporting and securely storing $CO_2$ underground in depleted oil and gas fields or deep saline aquifer formations. First, capturing technologies allow the separation of $CO_2$ from gases produced in electricity generation and industrial processes by one of three methods: pre-combustion capture, post-combustion capture and oxyfuel combustion.

$CO_2$ is then transported by pipeline or by ship for safe storage. According to KAPSARC (2012), the captured $CO_2$ through pipeline raises a lot of technical issue and specific standard have yet been implemented by the industry. For ship transport, few countries have a specific regulation in place but still in their infancy. Transportation by ship will require the building of liquefaction/gasification

infrastructures which will be governed by existing regulation of LNG industries (KAPSARC, 2012).

Later, $CO_2$ is stored carefully in selected geological rock formations or reservoir that are typically located several kilometers below the earth's surface. With carbon inventory of 50 times greater than the atmosphere (Stephen, 2010), the underground (subsea) is a prime candidate for storage of captured $CO_2$ so that it will remain isolated from the atmosphere.

## 2.3 CCS Plant Worldwide

In early 2010, the Global CCS Institute (GCCSI) reported that there were 80 large scale integrated CCS projects worldwide with different phase of development (KAPSARC, 2012). These consist of the entire CCS chain of $CO_2$ capture, transport and storage. The development of CCS project brought significant concern on the uncertainties to determine how much $CO_2$ being injected underground. However, general figures for total amount of $CO_2$ injected can be estimate from the two types of current injection projects (KAPSARC,2012); the Sleipner and Snohvit project in North Sea, Weyburn and Midale $CO_2$-EOR operation in Canada and injection project at In-Salah in Algeria which mostly involved in large-scale CCS application and the other that related to small-scale CCS and $CO_2$-EOR pilot injection at Zama in British Columbia, $CO_2$ injection at Lacq in France and Mountaineer Project in West Virginia.

According to Global CCS Institute (2015), all 22 large-scale CCS project either in operations or under construction have a collective $CO_2$ capture capacity of around 40 million tonnes (Mt) per year (IEA, 2015). The International Energy Agency (IEA), is an intergovernmental organization which specifically focused on mitigating climate change, has introduced Blue Map scenario strategies to reduce greenhouse gas emission by 50% by 2050. Meantime, the IEA Blue Map put a target for CCS project deployment require 100 projects by year 2020.

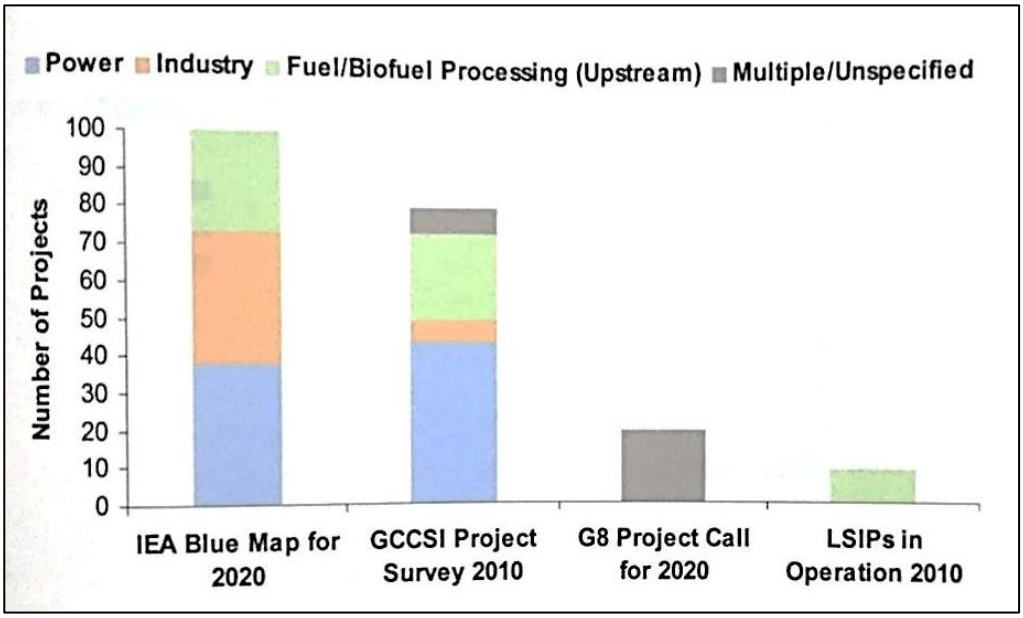


FIGURE 2.2 Comparison of various CCS deployment statistics (IEA, GCCSI)

This concludes that, the CCS project has grown dramatically due to the fact of tremendous climate change by rapid greenhouse gas emissions and the need for the reduction of the gas is significant. However, the advent of CCS project will result in $CO_2$ being handled in large volume which rise the public concern regarding the environmental risk associated with CCS, particularly the possibility of $CO_2$ leakage and their impact to the marine environment (Dewar et al., 2013a; Kita et al., 2015).

## 2.4 Subsea Release of $CO_2$

Rapid dissolution of $CO_2$ in seawater, caused by leakage results in a subsequent lowering of pH (Kita et al., 2015); increase in $pCO_2$ together with an increase in bicarbonate ions, decrease in carbonate ions and decrease of calcium carbonate saturation of seawater (Zeebe & Wolf-Gladrow, 2001) which may impact the marine organisms due to chemical alterations (Kita et al., 2015). All changes in $CO_2$ concentration is due to any biological process that dependent on bicarbonate or carbonate ion or change in pH (J. Blackford et al., 2013).

Dispersion of $CO_2$ in seawater is a complex process (J. C. Blackford, Torres, Cazanave, & Artioli, 2013). At the initial point of release, $CO_2$ will be released into the seawater which mostly in the liquid form. But, as heat is absorbed from surrounding water it will form mixture of gaseous $CO_2$ bubbles and possibly some

fine particles of solid $CO_2$ (Global CCS Institute, 2013). The density of both liquid and bubbles is lower than the seawater and they will start move upwards from the point of release. As it move upwards, some of the $CO_2$ will dissolve into the seawater and the rest will probably emerge at the surface as a relatively cold gas pool and dense $CO_2$ plume will tend to sink at the bottom (J. Blackford et al., 2013). $CO_2$ that dissolve in the seawater will form carbonic acid which then increases the local seawater acidity. Other than that, there are also potential $CO_2$ hydrates to form, which will capture $CO_2$ and released over a longer period of time as the hydrates absorbs heat from the surrounding seawater (Global CCS Institute, 2013). However, the phenomena described are not well understood nor have they been quantified (Global CCS Institute, 2013) and their impact in reducing the hazard associated with subsea leaks should be investigated more carefully.

## 2.5 Review of previous studies

There have been number of recent publications or studies examining the release and dispersion model of $CO_2$. Recent studies related to the released of $CO_2$ discussed about the bubble distribution, change in pH due to additional of $CO_2$ and study of carbonate system with respect to the leakage of $CO_2$. In other words, various model-based researches have been carried out recently to deploy the studies which discussed on the following paragraphs.

### 2.5.1 Bubble plume model

In order to study the effects of potential leak from CCS on the marine environment, The Quantifying and Monitoring Potential Ecosystem Impact of Geological Carbon Storage (QICS) project was launched to design a test monitoring methods, gain valuable experimental data and develop models to determine the change in dissolve inorganic carbon (DIC), pH and seawater $pCO_2$ through investigating the $CO_2$ bubble rising and dissolution characteristic (Dewar, Sellami, & Chen, 2015). The models are necessary to properly understand the characteristic of the leak point in terms of the gas phase plume and near field dissolved plume (Jones et al., 2015). Bubble sizes are the key determinant of the elevation of plume from the sea floor other than the pattern of dispersion and vertical profile of chemical change.

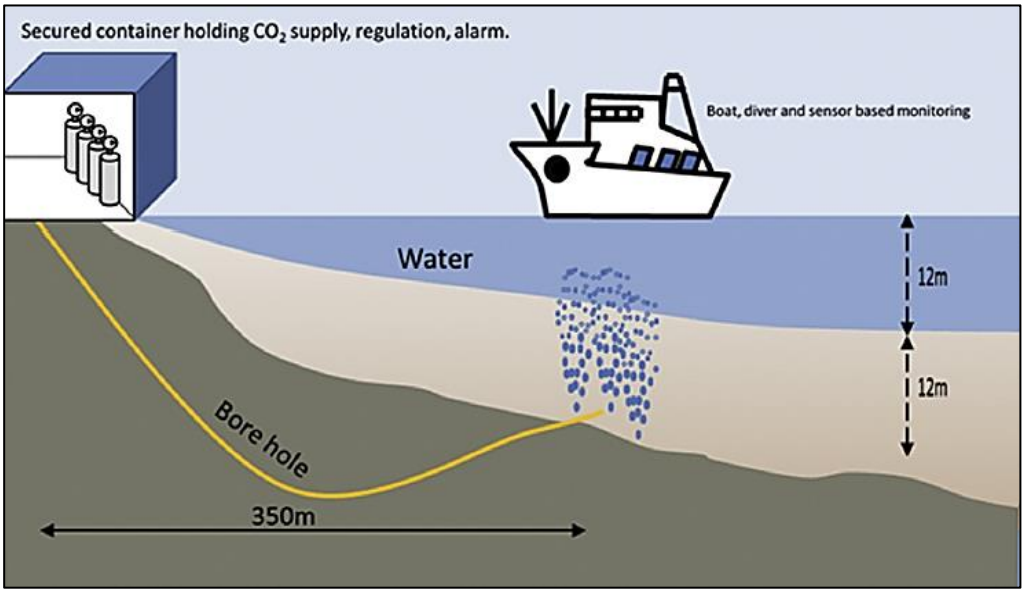


FIGURE 2.3 Schematic of QICS $CO_2$ release experiment

Previously, the QICS project used a novel controlled released of $CO_2$ into shallow subsea sediments (J. Blackford et al., 2015). Instead of focusing on the development of monitoring and observation methods, the project also generate experimental data to calibrate and develops model for predicting the change in pH or $pCO_2$ of the seawater in and above the sediments from leaked $CO_2$ (Dewar et al., 2015). The results showed, in very shallow water, only relatively small proportion (<15%) of gas injected below the seabed manifested as bubble plumes at the sea floor, and showed that bubble size and rise was highly sensitive to hydrostatic pressure (J. Blackford et al., 2015; Dewar et al., 2015; Sellami et al., 2015).

Based on the data obtained from QICS project, (Dewar et al., 2015) conducting an investigation on the dynamic characteristic of $CO_2$ bubbles in Scottish seawater using a mathematical model. It was found that most of the $CO_2$ bubbles deform to non-spherical bubbles observed near the seabed and the measured equivalent diameter are to be between 2mm to 12mm. The experiment approach were based on image processing program and video recording in order to measure the size and velocity of $CO_2$ bubbles. In order to examine the effects from seawater plume on the individual dynamics, two-phase plume model simulation were carried out in the second part of the study (Dewar et al., 2014) which aims to predict the fate of bubble plume by developing a sub-model in different setting against the data collected and

investigate the mechanism by comparing the measured impact of the leakage on water column in term of bubble plume and change in density of $CO_2$ during $CO_2$ injection. The volume of seawater with a given $pCO_2$ changes, would be the parameter to assess the impacts of leaked $CO_2$ on marine environment (Dewar et al., 2015).

### 2.5.2 Hydrodynamic model

Models that characterize the three dimensional (3D) movement and mixing of marine systems are the key components for understanding the dispersal of dissolve $CO_2$ (Jones et al., 2015).The hydrodynamic component of this modeling is provided by POLCOMS. A series of short-term and long-term leakage scenario were formulated to investigate the range of potential impact of geological $CO_2$ release. Realistic atmospheric, tidal and geostrophic forcing is essential in order to correctly estimate dispersion characteristics. The prediction of acidification is considered within the contact of variability of pH in the North Sea. As stated in the paper, eventhough the acidification due $CO_2$ leakage would be in addition to natural variability, the rate of acidification would be considerably faster than the long-term trend associated with rising atmospheric $CO_2$ (Phelps et al., 2015).

The results of the investigation are in good agreement with Blackford et al. (2008), but the improvement in the model conducted conveyed some differences in the local pH perturbations. For example, in Blackford et al. (2008) long term seepage scenario clearly state that the perturbations to pH reached maximum of 0.12 pH, whereas the study conducted by Phelps et al. (2015) present the perturbations exceeding 1 pH unit at the seabed. This may be caused by the improvement of model resolution; the volume of seawater receiving the $CO_2$ approximately doubles the volume from previous study, and as the results $CO_2$ concentration are much more significant thus cause highly reduction of local pH. This has also support previous dissertation where at initial studies leakage used available models, often with a relatively coarse resolution (~7km horizontal resolution) (Blackford et al., 2008) and were only able to address large scale leakage events. In present studies, resolution was improved as a result of advances in computational system. Model can now reach resolution of 1km horizontally (Phelps et al., 2015).

### 2.5.3 Carbonate system model

It is an essential component of all leakage simulations as they can derive pH, $pCO_2$, $CO_3^{2-}$and $HCO^{3-}$ion concentration and saturation state from given concentrations of dissolved $CO_2$(Jones et al., 2015). The carbonate system model have been available for decades, since 2005 international agreement on the parameterization of reaction constant (Dickson et al.,2007) and a far better treatment of alkalinity (e.g. Artioli et al., 2012) has improved the realism of these models, especially when applied to shelf and coastal systems. The study conducted by Phelps et al. (2015) recently is stimulated using an iterative speciation model based on HALTAFALL as applied in Blackford and Gilbert (2007), Blackford et al. (2008) and Artioli et al. (2012) with dissolved inorganic carbon (DIC) and total alkalinity (TA) as master variables.

Phelps et al. (2015) stated that, it is difficult to precisely determine on how the carbonate system react to the $CO_2$ leakages (under the environmental conditions) when the CCS is conducted in larger scale. It is because strong seasonal thermoclines are able to reduce the $CO_2$ exchange between the surface (or bottom) of the water which indirectly prevent outgassing of $CO_2$ to the atmosphere (Phelps et al., 2015). For example, the shallow depth in the North Sea site and strong tidal ensure the $CO_2$ to readily escape to the atmosphere compare the area in South Sea which considerably less sensitive to $CO_2$ addition. Thus, there is a need for further study to focus on the response of carbonate system to $CO_2$ leakages under projected future climate conditions, local conditions of different locations and depth where the study is applicable.

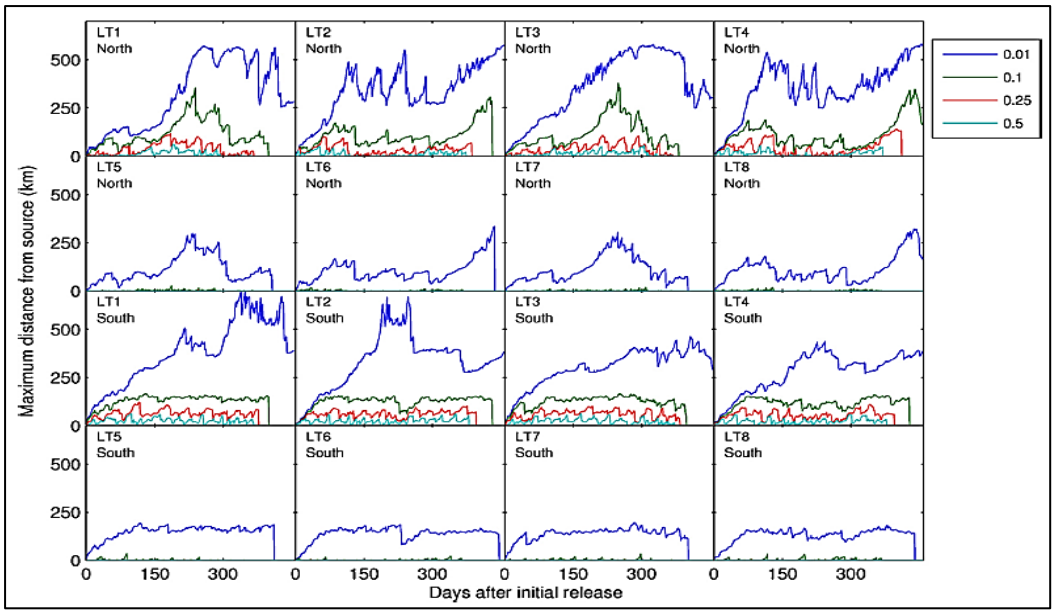


FIGURE 2.4 Greatest distance of four critical pH perturbation contours from the source over time for long-term leakage simulation (Phelps, Blackford, Holt, & Polton, 2015)

## 2.6 Selection of Model and Justification

The risk and environmental impact assessment related to $CO_2$ leakage are subjected into different type of dispersion model or numerical model which required further validation. However, the source of information or actual measurement from ongoing CCS demonstration projects are limited (Hvidevold, Alendal, Johannessen, & Mannseth, 2012). With regards to the need of the projects , the QICS release experiment can be considered as the most realistic representation for a small-leakage event that has so far been studied (Kita et al., 2015).

All models have its own uncertainties in the model output. However, such uncertainties is very challenging to assess and complexity of the model indirectly increase the challenge (Hvidevold et al., 2012). Among the three different models that have been discussed, the bubble plume model seems to be more critically required to be carried out with support from several numerical model available and existing experimental data which can easily be obtained.

There are a number of studies focused on the bubble plume model with majority used the experimental results from QICS projects. However, in current stage most of the modeling exercises are mathematical-based model and there are only few that used CFD modeling in their studies. CFD-based model are highly recommended to obtain more accurate picture of studies of potential hazards (Global CCS Institute, 2013). The $CO_2$ bubble plume model is one of the approach that can describes the momentum and mass transfer mechanism in seawater (Chen, Nishio, Song, & Akai, 2009). The parameter which also incorporated with the bubble plume model is the leakage depth which deploys the bubble behavior (velocity, size and etc.) in sea water. Other than that, the change in pH and density of $CO_2$ in seawater also can be analyze and simulated through the model. As once $CO_2$ bubble rises upwards from the seafloor, they grow in size and the density will decrease with respect to the decrease in pressure (Dissanayake et al., 2012).

A $CO_2$ seep to marine water will produce individual rising if between ~3000m and 500m, and bubbles if shallower than ~500m (Brewer at al., 2002). The dissolution of $CO_2$ content in the droplets of bubble will gradually acidify (drop or reduction in pH) the surrounding water (Caramanna, Andre', Dikova, Rennie, & Maroto-Valer, 2014). The environmental impacts due to the acidification, depends on how fast the bubbles dissolve and how fast the $CO_2$ concentration is diluted by local currents and mixing (Hvidevold et al., 2012). At first, the impacts of $CO_2$ bubble diffusion from small $CO_2$ leak (bubble/droplet) might be seen as undetectable but if maintained for long enough, the effect could potentially give a major impact to the marine organism. An accurate estimation of $CO_2$ seep in seawater is vital in assessing the subsequent consequence of any potential of $CO_2$ leakage.

Therefore, this project will discuss the study of $CO_2$ bubble rising into the surrounding water, by validating the experimental data and mathematical model that have been developed to investigate the consequences of $CO_2$ leakage to the marine ecosystem using CFD approach.

## 2.7 Theory for Modeling Dynamic of rising $CO_2$ bubble

Chen et al. (2005) develop a correlation of two phase model to stimulate the leakage of dynamic $CO_2$ bubble plume in QICS experiment based on the Eulerian-Eulerian droplet (Dewar et al., 2015). Then to solve two phase bubble plume, the modeling can be solved using the continuity and Navier-Stokes equation. The $CO_2$ bubble plumes are considered using the dissolution from mass transfer and momentum transfer. The plumes are referred to as dispersed phase and seawater carrier phase with void fraction $\alpha$.

$$\alpha_c + \alpha_d = 1 \tag{1}$$

The small scale turbulent ocean is modeled and reconstructed by means of large eddy simulation (LES) (Hirabayashi et al., 2012 ; Chen et al., 2005,and Alendal & Drange, 2001) and the governing equation for seawater carrier can be describe as:

$$\frac{\partial \bar{\rho}}{\partial t} + \frac{\partial \bar{\rho} u_i}{\partial x_i} = \dot{w}_{co2} \tag{2}$$

$$\frac{\partial \bar{\rho} u_i}{\partial t} + \frac{\partial \bar{\rho} u_i u_j}{x_j} = \frac{\partial \hat{p}}{\partial t} + \frac{\partial D_{ij}}{\partial x_i} + (\bar{\rho} - \rho_o)g + \dot{F} \tag{3}$$

$$\frac{\partial \bar{\rho} \widehat{\emptyset_c}}{\partial t} + \frac{\partial \bar{\rho} \widehat{\emptyset_c} u_j}{\partial x_j} = \frac{\partial}{\partial x_j}\left(\bar{\rho} D_k \frac{\partial \widehat{\emptyset_c}}{\partial x_j}\right) + \frac{\partial \bar{\rho} \hat{q}_k}{\partial x_j} + \dot{w}_{co2} \tag{4}$$

Governing equation for dispersed bubble;

$$\frac{\partial \hat{n}_d}{\partial t} + \frac{\partial \hat{n}_d u_{di}}{\partial x_i} = \hat{q}_{dn} \tag{5}$$

$$\frac{\partial \hat{\alpha}}{\partial t} + \frac{\partial \hat{\alpha} u_{dj}}{\partial x_j} = \hat{q}_{dco2} - \frac{\dot{w}_{co2}}{\rho_d} \tag{6}$$

$$\frac{\partial \bar{\rho}_d u_{dj}}{\partial t} + \frac{\partial \bar{\rho}_d u_{di} u_{dj}}{\partial x_j} = \alpha(\bar{\rho}_d - \rho_w)g + \dot{F} \tag{7}$$

Sub-models for mass and momentum exchange are required to solve the governing equation (Dewar et al., 2013a) ;

$$\dot{w}_{co2} = \frac{3.0}{2.0}\left(\frac{\pi}{6.0}\right)^{\frac{1}{3}} \hat{\alpha}^{\frac{2}{3}} \hat{n}^{\frac{1}{3}} \frac{\pi}{d_{eq}} Sh D_f (C - C_O) \tag{8}$$

$$\dot{F} = 0.75\,(\frac{\pi}{6.0})^{\frac{1}{3}}\,\rho_d\,\hat{\alpha}^{\frac{2}{3}}\,\hat{n}^{\frac{1}{3}}C_d|u_j - u_{dj}|(u_j - u_{dj}) \tag{9}$$

Where equation (8) and (9) are the mass exchange from $CO_2$ dissolution and momentum exchange term of the drag force between bubble and seawater respectively.

Drag coefficient is required to describe how drag changes with seawater at a given size and shape of the bubbles. Therefore, a best fit model is proposed from (Bigalke et al., 2008;2010) that convert velocity and diameter data to Reynolds number and drag coefficient using (Clif's et al., 1978) equation for terminal velocity;

$$C_d = \frac{24}{Re} f(Re) \tag{10}$$

Where f(Re) is

$$f(Re) = 1 + 0.045Re - 1.50 \times 10^{-4}Re^2 + 3.20 \times 10^{-7}Re^3 \tag{11}$$

But this correlation is valid for Re up to 400 and beyond that the sub-model from Bozzano and Dente (2001) is employed;

$$C_d = f\left(\frac{a}{R_o}\right)^2 \tag{12}$$

Where f is the friction factor and can be define as

$$f = \frac{48}{Re}\left(\frac{1 + 12M^{\frac{1}{3}}}{1 + 36\,M^{\frac{1}{3}}}\right) + 0.9\left(\frac{E_o^{\frac{3}{2}}}{1.4\,\left(1 + 30M^{\frac{1}{6}}\right) + E_O^{\frac{3}{2}}}\right) \tag{13}$$

While the deformation factor $\left(\frac{a}{R_o}\right)^2$ can be define as

$$\left(\frac{a}{R_o}\right)^2 = \frac{10 + \left(1 + 1.3\,M^{\frac{1}{6}}\right) + 3.1E_o}{10 + \left(1 + 1.3\,M^{\frac{1}{6}}\right) + E_o} \tag{14}$$

For mass exchange through dissolution the equation developed by Clift et al. (1978) and Johnson et al. (1969), Sherwood Number, Sh ( ratio of convective to diffusive exchange) can be used.



(15)

$$\mathrm{Sh} = \frac{\mathrm{d_{eq}}}{\mathrm{D_f}}\mathrm{k}$$

The equation can describe how shape, size and flow will affect dissolution rate (Dewar et al., 2013a). The mass transfer coefficient, k(m/s) can vary depending on bubble diameter and velocity ;

$$\mathrm{k} = \mathrm{f_k}(\mathrm{d_{eq,}}\mathrm{u_d}) \times \mathrm{D_f}^{0.5} \tag{16}$$

Where $f_k(d_{eq,}u_d)$ varies dependent on bubble diameter.

$$\mathrm{f_k}(\mathrm{d_{eq}}, \mathrm{u_d}) = \begin{cases} 1.13\,(\frac{\mathrm{u_d}}{0.45+20\mathrm{d_{eq}}})^{0.5}, & \mathrm{d_{eq}} < 5\mathrm{mm} \\ 6.5, & 5\mathrm{mm} < \mathrm{d_{eq}} < 13\mathrm{mm} \\ \frac{0.219462}{\mathrm{d_{eq}}^{0.25}}, & \mathrm{d_{eq}} > 13\mathrm{mm} \end{cases} \tag{17}$$

The initial bubble size or equivalent diameter is important to determine the rate of $CO_2$ dissolution and rises while the buoyancy and drag being the major force controlling dynamic (Dewar et al., 2013a). The force balance is used to predict the bubble size as defined below;

$$\left[(\rho_w - \rho_{CO_2})g\frac{\mathrm{d_{eq}}^3}{6}\right]^2 + \left[\frac{\mathrm{C_d}}{8}\rho_w u^2 \mathrm{d_{eq}}^2\right]^2 = [\mathrm{d_{ch}}\sigma]^2 \tag{18}$$

According to Kulkarni and Joshi (2005), these correlations assume that, $CO_2$ bubble is dependent to the current and changes in the sediment wall until drag and buoyancy force exceed the tension between both across the seabed (Dewar et al., 2013a; Dewar, Wei, McNeil, & Chen, 2013b).

# CHAPTER 3

# METHODOLOGY

The methodology of the project in predicting the consequence of toxicity of $CO_2$ released will be carried out by working on the existing experimental data that was obtained from recent studies. A comparison studies and validation of other developed model to the CFD approach will be highlighted in this dissertation. The dispersion model using commercial CFD code, ANSYS-FLUENT is proposed to predict consequences of bubbles $CO_2$ release into the seawater.

Computational fluid dynamics (CFD) widely used to study the variety of gas release and dispersion model. The CFD techniques can predict the gas concentration at any point and time inside the computational domain with the ability to stimulate both ideal and realistic conditions (Zhang & Chen, 2010). The study that will be conducted will take the basis of existing mathematical modeling and the result will be validated using the CFD approach, through Ansys Fluent software. This may not be an ideal way of validating a model; however a very little experimental data are available for the release and dispersion of $CO_2$ bubble in seawater.

## 3.1 Modeling

### 3.1.1 Multiphase model

The term of Multiphase model is used to refer to any fluid flow consisting more than one phase or component (Hassan, 2014). General multiphase model are available in Ansys Fluent software that can be used to simulate different multiphase flow regimes. In this project, the gas-liquid multiphase regimes are evaluated using Eulerian Model.

The Eulerian Model comes with tools where the interphase drag coefficient function can be modified through user-defined functions (ANSYS,2013).The equations solve by the software can defined the concept of phasic volume fraction, mechanism of momentum and mass between the phases.

**i. Volume fraction equation**

Volume fraction represents the space occupied by each phase and the laws of conservation of mass and momentum for the respective phase (ANSYS, 2013).

The volume of phase q, $V_q$ is defined as

$$V_q = \int_V \alpha_q dV \tag{19}$$

Where $\sum_{q=1}^{n} \alpha_q = 1$

The effective density of the phase q is, $\rho_q = a_q \rho_q$, with $\rho_q$ is the physical density of phase q.

The volume fraction was solved through implicit discretization method, where a standard scalar transport equation is solved iteratively for the secondary phase ($CO_2$) volume fraction for every time step.

**ii. Conservation of Mass and Momentum**

The continuity equation for phase q,

$$\frac{\partial}{\partial t}(\alpha_q \rho_q) + \nabla.(\alpha_q \rho_q \vec{V}_q) = \sum_{\rho=1}^{n} (\dot{m}_{pq} - \dot{m}_{qp}) + S_q \tag{20}$$

The momentum balance for phase q yields

$$\frac{\partial}{\partial t}(\alpha_q \rho_q \vec{V}_q) + \nabla.(\alpha_q \rho_q \vec{V}_q \vec{V}_q) = -\alpha_q \nabla_\rho + \nabla.\bar{\bar{\tau}}_q + \alpha_q \rho_q \vec{g} + \sum_{\rho=1}^{n} (\vec{R}_{pq} + \dot{m}_{pq}\vec{V}_{pq} - \dot{m}_{qp}\vec{V}_{qp}) + (\vec{F}_q + \vec{F}_{lift,q} + \vec{F}_{wl,q} + \vec{F}_{vm,q} + \vec{F}_{td,q}) \tag{21}$$

Where $\bar{\bar{\tau}}_q$ is the stress-stain tensor at $q^{th}$ phase.

### 3.1.2 Turbulence Model (Standard k-$\varepsilon$ Model)

The standard k-$\varepsilon$ model is a model based on model transport equations for the turbulence kinetic energy (k) and its dissipation rate ($\varepsilon$). The model transport equation for k is derived from the exact equation, while the model transport equation for $\varepsilon$ was obtained using physical reasoning and bears little resemblance to its mathematically exact counterpart. The following transport equations used to find the turbulence kinetic energy (k) and its dissipation rate ($\varepsilon$).

$$\frac{\partial}{\partial t}(\rho k) + \frac{\partial}{\partial x_i}(\rho k u_i) = \frac{\partial}{\partial x_j}\left[\left(\mu + \frac{\mu_t}{\sigma_k}\right)\frac{\partial k}{\partial x_j}\right] + G_k + G_b - \rho\varepsilon - Y_M + S_K \quad (22)$$

and

$$\frac{\partial}{\partial t}(\rho\varepsilon) + \frac{\partial}{\partial x_i}(\rho\varepsilon u_i) = \frac{\partial}{\partial x_j}\left[\left(\mu + \frac{\mu_t}{\sigma_\varepsilon}\right)\frac{\partial \varepsilon}{\partial x_j}\right] + G_{1\varepsilon}\frac{\varepsilon}{k}(G_k + G_{3\varepsilon}G_b) - G_{2\varepsilon}\rho\frac{\varepsilon^2}{k} + S_\varepsilon \quad (23)$$

### 3.1.3 Population Balance model

The Population Balance Model (PBM) is used for the modeling of $CO_2$ bubble rising in seawater. The parameter such as the size distribution of bubble particles, bubble dissolution and dispersion can be comprehensively evaluated. All of the parameter used with combination of transport and chemical reaction in a multiphase system that required describing change in particle population in addition to momentum and mass balance.

PBM is very useful to predict the phenomena such as coalescence, nucleation and breakage of bubble or droplet and size distribution of particle in flow regime. Other than that, the approach also can describe the variation in particle population and extent of particle influencing of fluid flow.

#### i. Particle state vector

The particle state vector is characterized by a set of external and internal coordinate. The coordinate is denoted as a number of density functions.

Total number of particles of entire system is defined as;

$$\int_{\Omega_\emptyset} \int_{\Omega_{\vec{x}}} n dV_{\vec{X}} dV_\emptyset \tag{24}$$

The local average number density in physical space (the total number of particles per unit volume of physical space) denoted by;

$$N(\vec{x}, t) = \int_{\Omega_\emptyset} n dV_\emptyset \tag{25}$$

The total volume fraction of all particles is given by;

$$a(\vec{x}, t) = \int_{\Omega_\emptyset} nV(\emptyset) dV_\emptyset \tag{26}$$

Where the volume of single particle can be calculated as;

$$V = \frac{\pi}{6} L^S \text{, where (L is the diameter of the particle)} \tag{27}$$

### ii. Population Balance Equation (PBE)

Assuming that $\varphi$ is the particle volume, then the PBE can be written as;

$$\frac{\partial}{\partial t}[n(V,t)] + \nabla.[\vec{u}n(V,t)] + \underbrace{\nabla_v.[G_v n(V,t)]}_{\text{Growth term}} = \frac{1}{2}\int_0^V \underbrace{a(V-V', V')n(V-V', t)n(V', t)\, dV'}_{\text{Birth due to aggregation}} - \int_0^\infty a(V, V')n(V, t)n(V', t)dV' + \int_{\Omega_V} \underbrace{pg(V')\beta(V|V')n(V', t)dV'}_{\text{Birth due to breakage}} - \underbrace{g(V)n(V,t)}_{\text{Death due to breakage}}$$

(28)

### iii. Discrete method

Discrete method was chosen to simulate the PBM because it can discretize the particle population into a finite number of size intervals. It is useful for computing the particle size distribution (PSD) directly. It

was found from the data obtained by the experiment, the size of the leaked $CO_2$ bubble are between 0.2cm and 1.2cm (Sellami et al., 2015). Therefore by using the discrete approach, the population of the bubble can be discretized to relative number of size intervals and the size distribution that is coupled with fluid dynamics can be computed (ANSYS, 2013).

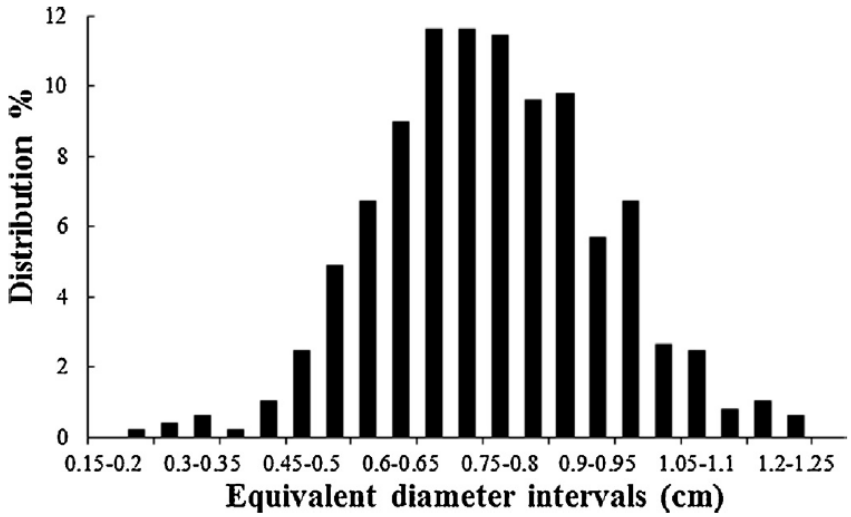


FIGURE 3.1 Size distribution of leaked $CO_2$ bubble obtained from the experiment (Sellami et al., 2015).

## 3.2 Case studies

The simulation of QICS experiment performed by Dewar et al. (2014) examined in the model considering the three injection rates at the early, middle and late stage of the experiment; 80 kg/day, 170kg/day and 208kg/day respectively. As the injection rate increases during the experiment, the leakage rate also increases. However, the leakage rates for $CO_2$ from the seabed are difficult to estimates. Therefore a prediction based on the type of leak and the location it occurs is the most data that can be evaluated (Dewar et al., 2013b). The leakage rates were predicted to be 2.3kg/day, 17.0kg/day and 31.2 kg/day (Dewar et al., 2015). The data are used in this study for model validation by considering the scenario at the worst case conditions only; refers to the highest injection rate of 208kg/day with subsequent $CO_2$ leakage rates of 31.2kg/day.

The case studies used the case modeling of shallow depth leakage prediction based on QICS experiment that mapped the seawater to be at low and high tides of 9.5m and 12m depth respectively (Dewar et al., 2015). The leakage distances are taken as the approximate size of the pockmarks after leakage of $CO_2$ from seabed. The pockmarks locations are determined based on the study done by Dewar et al. (2014).

To examine the bubble dissolution in seawater, consideration of mass and momentum transfer as well as the force acting through the bubble is essential. The scenario demonstrates the bubble are free rising in the seawater thus the force acting on the bubble are mainly drag and lift (buoyancy) force only.

### 3.2.1 Mass transfer

For each mass transfer mechanism, the population balance was chosen. It will allow for modeling a flow where a number density function is introduced to account for the particle population. With the aid of particle properties (such as particle size, porosity and etc.) different particles in the population can be distinguished and their behavior can be described.

### 3.2.2 Drag and Lift force

Grace et al. model and Tomiyama lift force model are used for the consideration of drag and lift force.

#### i. Grace et al. Model

The Grace model is well suited to gas-liquid flows which the bubble can have range of shapes. According to Reidun (2004), the Grace model take into account a varying shape by including the dimensionless numbers; Morton number (Mo), Eotvos number(Eo) and Reynolds number (Re) in the theories of dynamic

$$f = \frac{C_D\,Re}{24} \tag{29}$$

$$Re = \frac{\rho_q|\vec{v}_p - \vec{v}_q|d_p}{\mu_q} \tag{30}$$

$$C_D = \max(\min(C_{D-ellipse,} C_{D-Cap}), C_{D-Sphere})$$

$$C_{D-sphere} = \begin{cases} \frac{24}{Re}, & Re < 0.01 \\ \frac{24(1+0.15Re^{0.687})}{Re}, & Re \geq 0.01 \end{cases} \quad (31)$$

$$C_{D-cap} = \frac{8}{3} \quad (32)$$

$$C_{D-ellipse} = \frac{4}{3}\frac{gd_p}{U_t^2}\frac{(\rho_q - \rho_p)}{\rho_q} \quad (33)$$

Where

$$U_t = \frac{\mu_q}{\rho_q \mu_q} Mo^{-0.149}(J - 0.857) \quad (34)$$

Where Mo is the Morton number given by

$$Mo = \frac{{\mu_q}^4 g\,(\rho_q - \rho_p)}{\rho_q^2 \sigma^3} \quad (35)$$

J is given by piecewise function:

$$J = \begin{cases} 0.94H^{0.757}, & 2 < H < 59.3 \\ 3.42H^{0.441}, & H > 59.3 \end{cases} \quad (36)$$

$$H = \frac{4}{3} EoMo^{-0.149}\left(\frac{\mu_q}{\mu_{ref}}\right)^{-0.14}$$

Eotvos number is

$$Eo = \frac{g\,(\rho_q - \rho_p)d_p^2}{\sigma} \quad (37)$$

and $\mu_{ref} = 0.0009\ kg/(m - s)$

**ii. Tomiyama Lift force model**

In the multiphase flow, the lift forces are mainly act on the secondary phase ($CO_2$) of the fluid. The lift forces are applied because of the velocity gradients in the primary phase (seawater) flow field. The Tomiyama Lift force model is used as it applicable to the lift force on

larger-scale deformable bubbles in the ellipsoidal and spherical cap regime. This model is dependent on the Eo number.

$$C_l = \begin{Bmatrix} \min[0.288\tanh(0.121Re_p), f(Eo')] & Eo' \leq 4 \\ f(Eo') & 4 < Eo' \leq 10 \\ -0.27 & 10 < Eo' \end{Bmatrix} \quad (38)$$

$$f(Eo') = 0.00105Eo'^3 - 0.0159Eo'^2 - 0.0204Eo' + 0.474$$

$Eo'$ is a modified Eotvos number based on the long axis of the deformable bubble, $d_h$ :

$$Eo' = \frac{g(\rho_q - \rho_p)d_h^2}{\sigma} \quad (39)$$

$$d_h = d_b(1 + 0.163Eo^{0.757})^{1/3}$$

$$Eo = \frac{g(\rho_q - \rho_p)d_b^2}{\sigma} \quad (40)$$

Where $\sigma$the surface tension, g is is the gravity and $d_b$ is the bubble diameter.

Therefore the Grace et al. model and Tomiyama lift force model could then possibly be used for this study. It also depict the mathematical modelling by (Sellami et al., 2015) as they used dimensionless numbers Mo, Eo and Re to characterise the motion and shape of $CO_2$ bubble in their calculations.

## 3.3 Computational domain and mesh system

### 3.3.1 Geometry

The construction of the geometry depicts the case study of the model. A 2D geometry was built for the $CO_2$ release scenario in seawater at low and high tides condition. In the construction of the geometry, the boundary conditions are specified as;

i. **$CO_2$ inlet** at the leakage point of $CO_2$ in seawater
ii. **Seawater inlet** for the surrounding water (free rising of $CO_2$)
iii. **Outlet** is the sea surface (atmosphere)

iv. **Wall1** and **Wall2** are the seabed (assume as a non-slip boundary)

v. **Symmetry** for the open surface in seawater

The two dimensional computational domain and $CO_2$ leakage sites are set up as the following figures;

i. Low tides (9.5m)

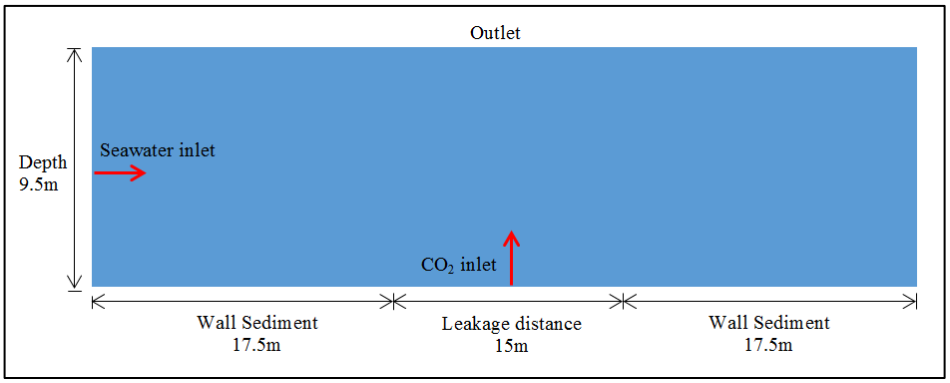


FIGURE 3.2 Computational domain at low tides

ii. High tides (12m)

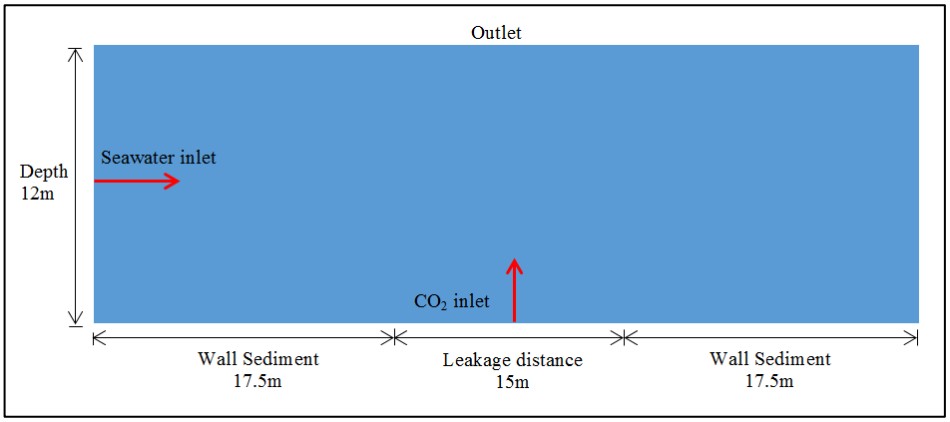


FIGURE 3.3 Computational domain at high tides

### 3.3.1 Meshing

Meshing was done right after the completion of geometry for the model. It is required in order to yield an accurate display of the results. The meshing mode is run in a double precision mode. A two dimensional mesh system is used for the analysis. The mesh is in horizontal and vertical direction with non-uniform grid distribution.

An increase in mesh number will improve the resolution of the model (Dewar et al., 2013b). The mesh setups for each scenario are listed in table below;

TABLE 3.1. Grid number for the mesh setup

| Case study | Grid number | | | |
|---|---|---|---|---|
| | $CO_2$ inlet | Seawater inlet | Outlet | Wall (sediment) |
| $CO_2$ leak at low tides (9.5m) | 80 | 50 | 200 | 80 |
| $CO_2$ leak at high tides (12m) | 80 | 90 | 200 | 80 |

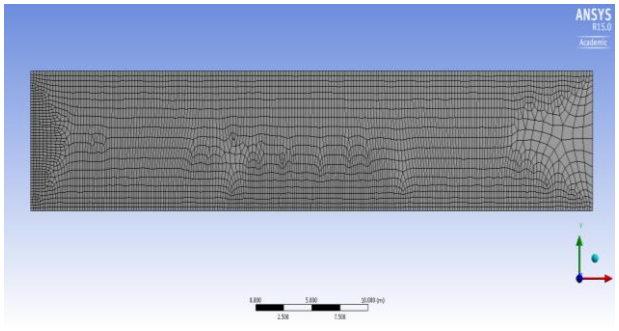


FIGURE 3.4 Meshing for low tides scenario

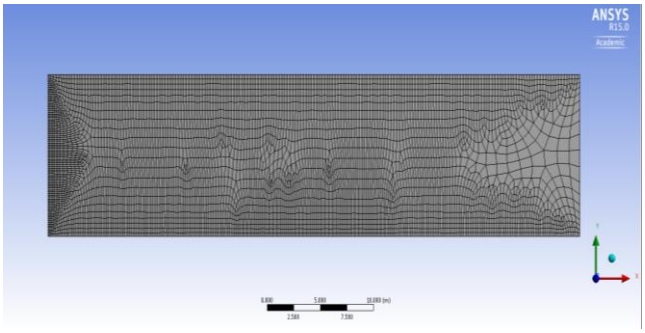


FIGURE 3.5 Meshing for high tides scenario

## 3.4 Physical Properties

The pockmarks location simulated by Dewar et al. (2014) is taken as the approximate size of the leakage occurring over 15m distance. The plume background seawater velocity data 0.05m/s is used to estimate the relative velocity of the observed bubbles (Sellami et al., 2015). The physical properties at ambient temperature of the seawater and $CO_2$ bubble are reported in table below;

TABLE 3.2. Physical properties of the seawater and $CO_2$ (Sellami et al., 2015)

| Properties | Seawater | $CO_2$ |
|---|---|---|
| Dynamic Viscosity (mPas) | 1.4 (Schetz and Fuhs, 1999) | 14.2 (National Bureau of Standards, 1960) |
| Interfacial tension (N/m) | $7.37 \times 10^{-2}$ (Chun and Wilkinson, 1995) | - |
| Density (Kg/m3) | 1027 (Unesco, 1981) | 1.9 (Ito, 1984) |
| Measured salinity (ppt) | 33.7 | - |

## 3.5 Setup Physics

### 3.5.1 General

Upon completion of the mesh, the geometry is run in ANSYS Fluent 16.0. The geometry is first checked in the fluent and the progresses are reported in the console. This is to ensure that the reported minimum volume is a positive number. The general setups for the solver are set as; density based, absolute velocity formulation, transient, 2D planar with gravitational force acting.

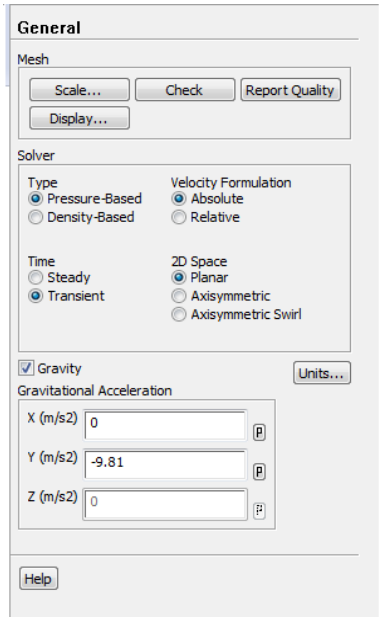


FIGURE 3.6 General setup

### 3.5.2 Model

a. Multiphase Model

For modeling setup, the multiphase, viscous turbulence and population balance model are used. The multiphase model was selected to simulate multiphase flow regime (fluid flow consisting two component; carbon dioxide and seawater). Eulerian model was selected from the model list.

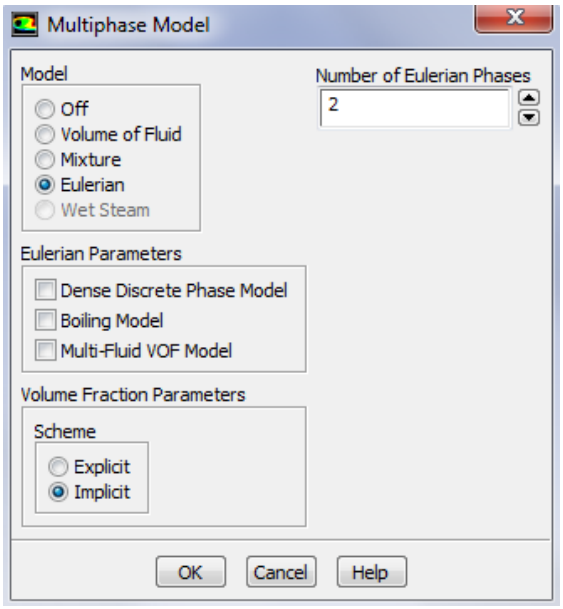


FIGURE 3.7 Multiphase model setup

b. Viscous Turbulence model

Next, turbulence model (standard k-$\varepsilon$ model) is used to model transport equation for the turbulence kinetic energy (k) and its dissipation rate ($\varepsilon$).

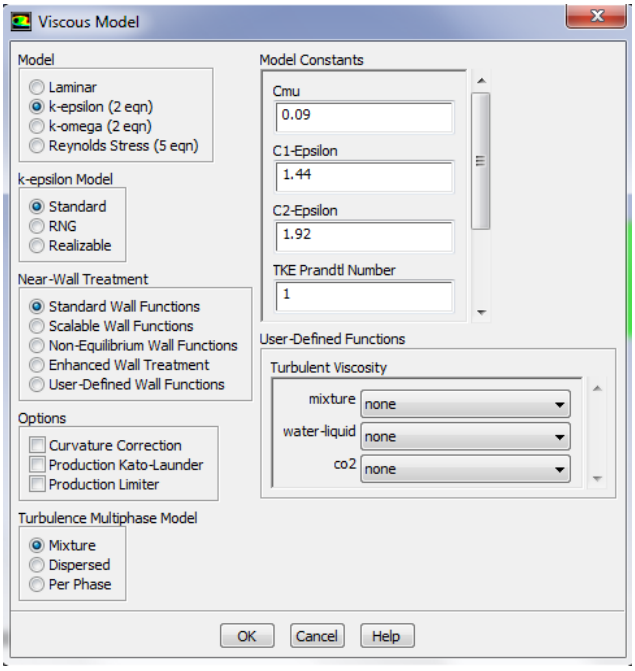


FIGURE 3.8 Viscous turbulence model setup

c. Population balance model

The population balance is used to describe the particle population of $CO_2$ bubble in seawater in addition to momentum and mass balance. Discrete method was chosen as it can discretize the particle population into finite number of size intervals. For phenomena, breakage and aggregation kernel are used to describe the birth and death of particles due to breakage and aggregation processes and for this purposes, Luo model are chosen from the drop-down list. Luo model is an integrated kernel that encompassing breakage frequency and define the aggregation in terms of rate of particle volume formation as a results of binary collision of the particles. The default breakage formulation for the discrete method in ANSYS Fluent is based on Hagesather method where the breakage sources are distributed to the respective size of bins, preserving mass and number density. Therefore, it is remain as it is. The surface tension requested by the model is remained as default value.

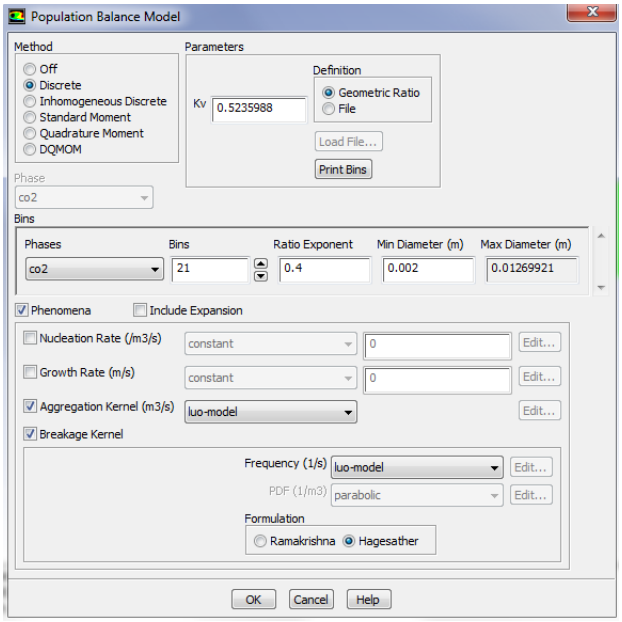


FIGURE 3.9 Population balance model setup

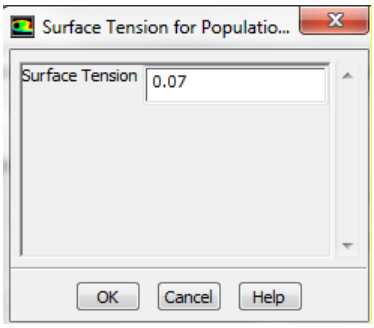


FIGURE 3.10 Surface tension for population balance model

### 3.5.3 Material

Materials are copied from the fluent materials database. For the simulation, seawater and carbon dioxide are chosen from the Fluent Fluid Material list. The properties of the material (i.e. density, viscosity) are set according to physical properties of the fluid based on QICS experiment.

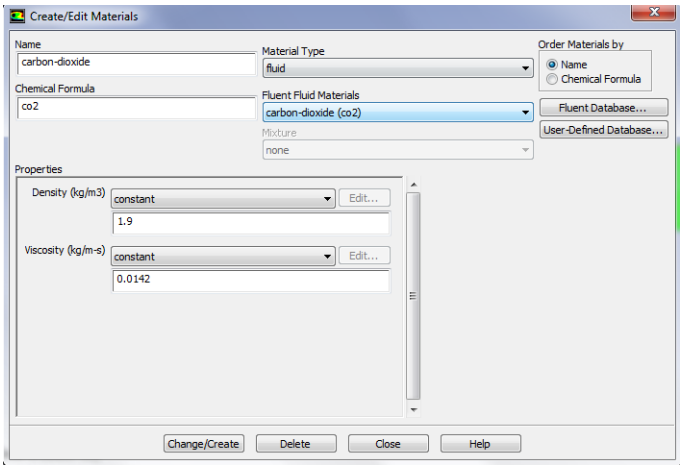


FIGURE 3.11 Properties of Carbon dioxide

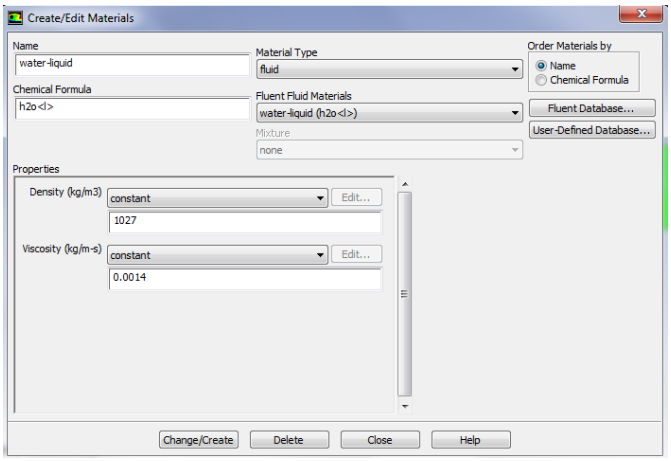


FIGURE 3.12 Properties of seawater

### 3.5.4 Phase

In the phase dialog box, the water-liquid is selected as Phase-1- Primary Phase and carbon dioxide selected as Phase-2- Secondary Phase. In the secondary phase dialog box, the diameter property changed automatically to sauter-mean once the population balance model is included. For the interaction, Grace et al. Model and Tomiyama Model are selected from the drop-down list for drag and lift force consideration. The Grace model is well suited to gas-liquid flows which the bubble can have range of shapes. The Tomiyama Lift force model is used as it applicable to the lift force on larger-scale deformable bubbles in the ellipsoidal and spherical cap regime. The default population balance option for mass transfer of $CO_2$ to seawater is selected to measure the mass transfer rate for the mixture. Lastly the surface tension is set as 0.0737 N/m according to physical properties for the selected fluid obtained from QICS experiment.

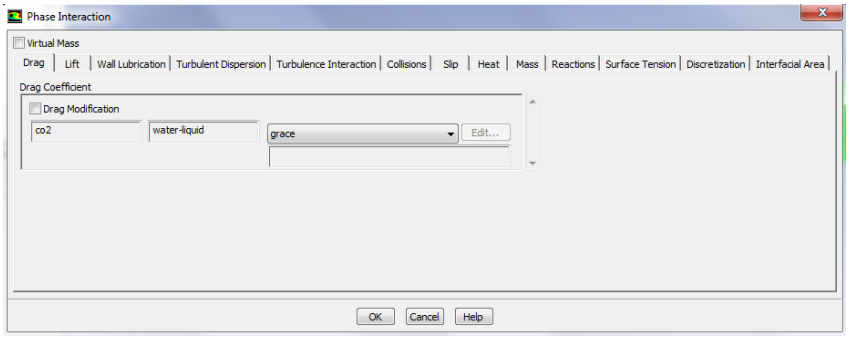


FIGURE 3.13 Drag force for phase interaction

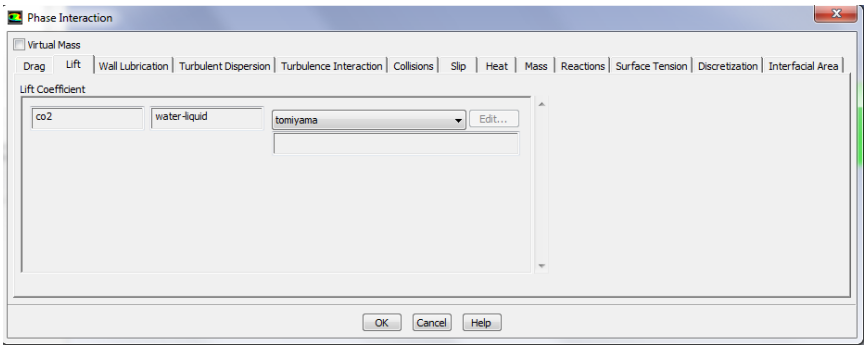


FIGURE 3.14 Lift force for phase interaction

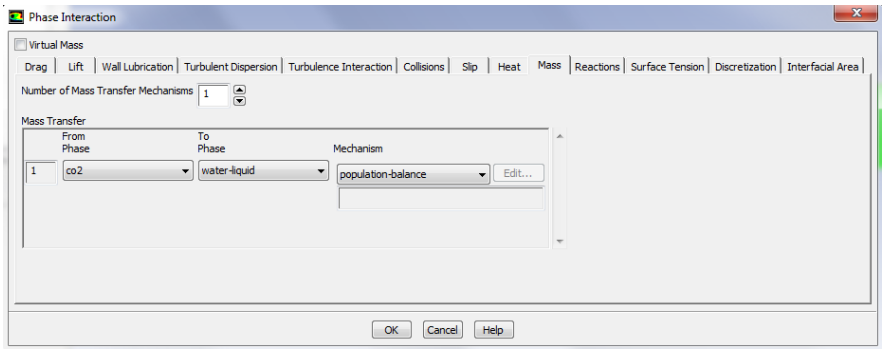


FIGURE 3.15 Mass transfer mechanism

### 3.5.5 Operating Conditions

For operating condition, gravity are enable and the gravitational acceleration is set as -9.81m/s2 in the Y direction. The specified operating density is set as 1027 kg/m3 for the operating density.

### 3.5.6 Boundary Conditions

a. Boundary condition at the inlet

i. $CO_2$ inlet

The mass flow rate of $CO_2$ release is set as 0.0003611 kg/s which is equivalent to 31.2kg/day. This value taken as the highest injection rate of $CO_2$ release based on QICS experiment. The K and epsilon was selected from the drop down list for turbulence

consideration in the mixture phase. Default value of the ANSYS fluent turbulence is remained as it is.

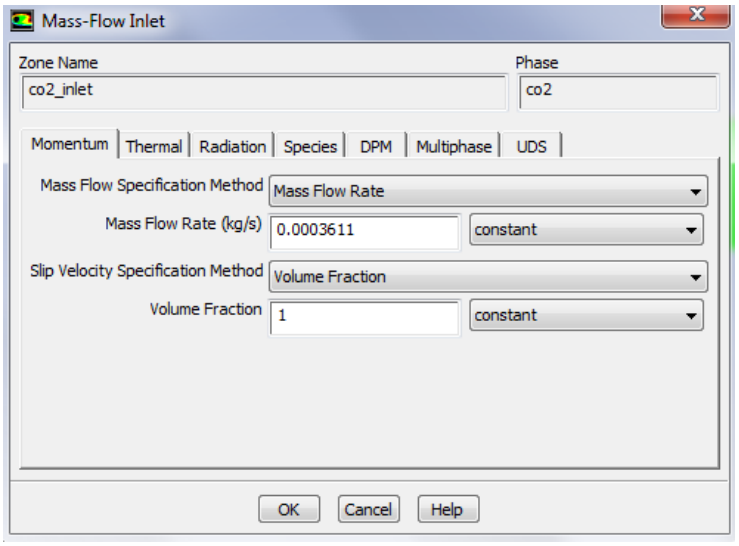


FIGURE 3.16 $CO_2$ inlet - Phase $CO_2$

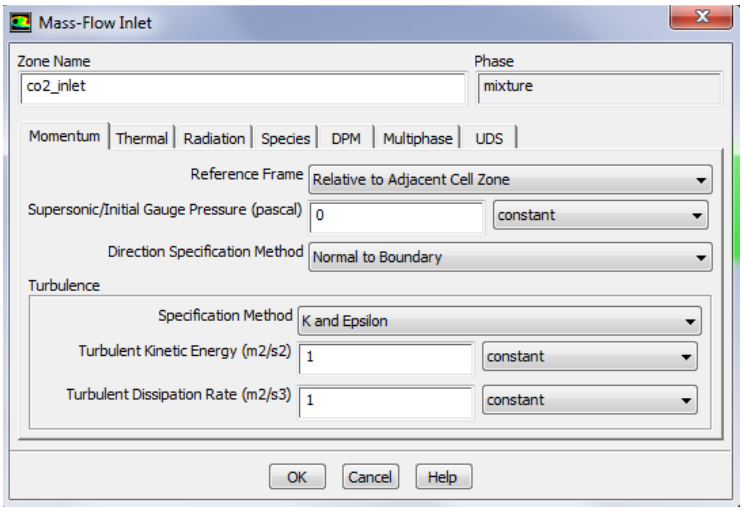


FIGURE 3.17 $CO_2$ inlet - phase mixture

ii. Seawater inlet

The background seawater velocity of 0.05m/s is obtained from the QICS experiment data. The turbulence considerations are set similar to $CO_2$ inlet boundary

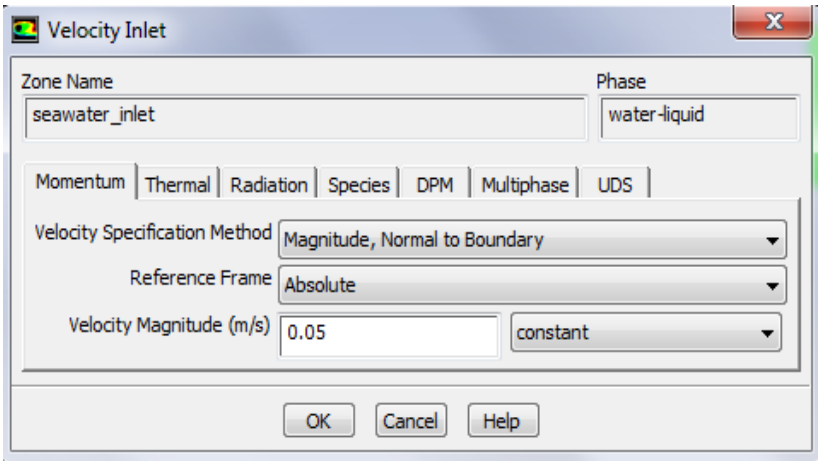


FIGURE 3.18 Seawater inlet- phase water liquid

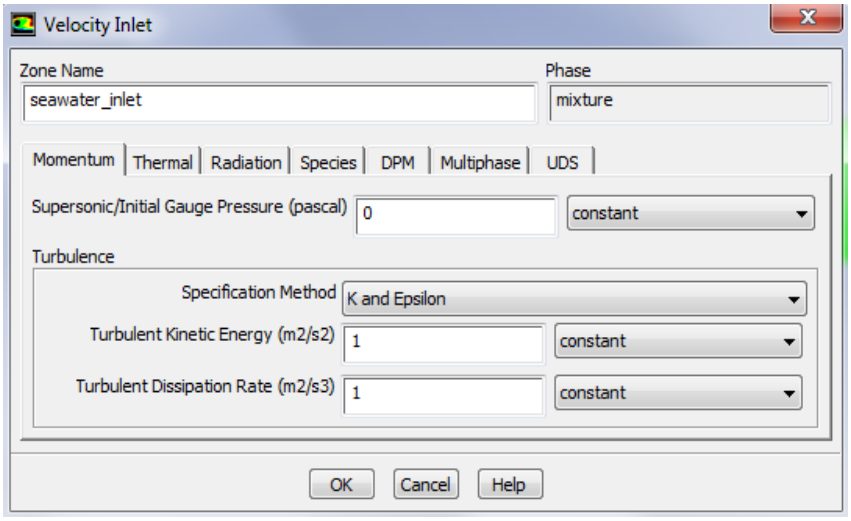


FIGURE 3.19 Seawater inlet- phase mixture

b. Boundary condition at the outlet

The boundary condition at the sea surface (outlet) is set as open boundary or in other means it is in atmospheric condition. Thus the outlet pressure is set as 101325 Pascal.

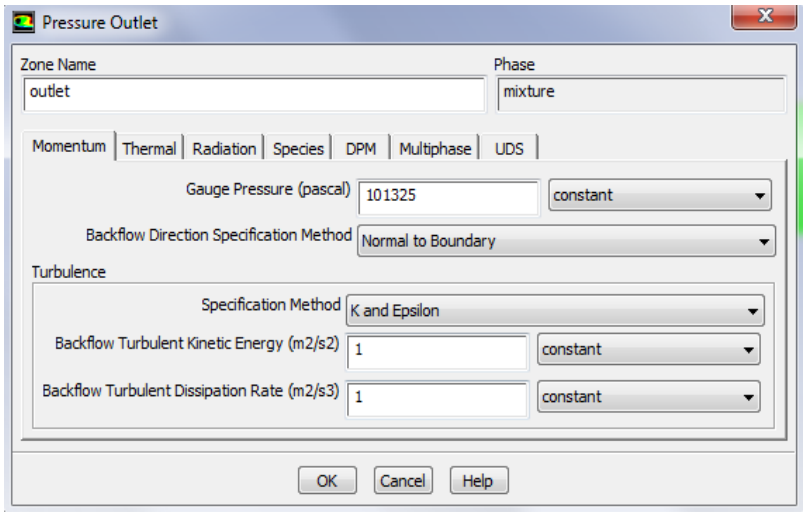


FIGURE 3.20 Outlet- phase mixture

### 3.5.7 Solution

a. Solution method

For the solution method, the phase coupled SIMPLE which is default setting of ANSYS Fluent is remains as it is. The default setting of Spatial Discretization parameter and Under Relaxation Factor parameter is retained.

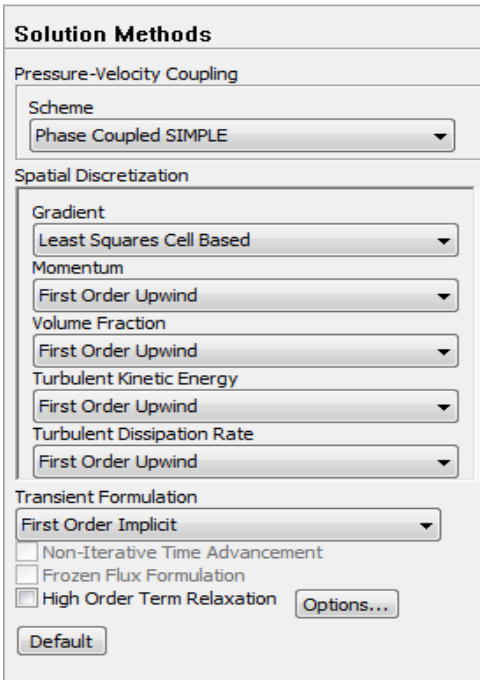


FIGURE 3.21 Solution method setup

b. Solution initialization

A hybrid initialization was chosen for simulation initialization. This option is selected as it displays a collection of boundary interpolation method. This option is beneficial as it can solve Laplace equation to determine the velocity and pressure fields. Other variables such as turbulence, species fraction, volume fraction and many more are automatically patched based on domain average values.


FIGURE 3.22 Solution initialization setup

c. Region adaption

Region adaption is necessary to avoid an overly dense mesh that probably create problem if the mesh if not fine enough to resolve the flow. The region based adaption is useful to refine the regions that intuitively require good resolution.

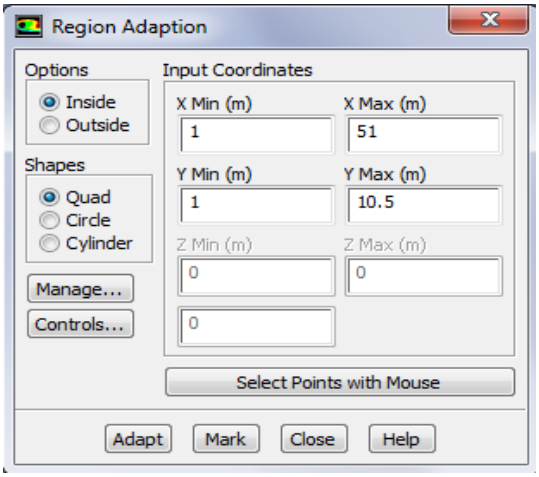


FIGURE 3.23 Region adaption setup for low tides release

### 3.5.8 Calculation

The simulation is modeled using time step of 1.5 following the setup of modeling by Dewar et al. (2015). The number time steps are calculated for 1 hour $CO_2$ release.

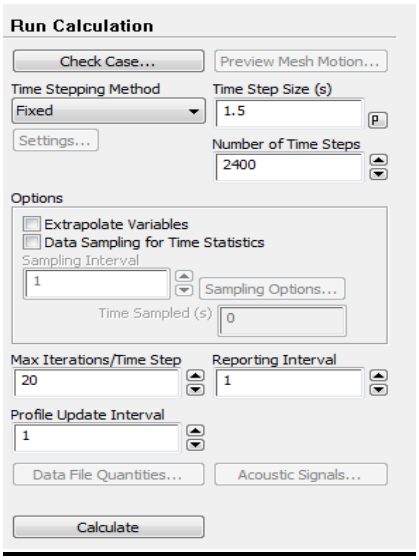


FIGURE 3.24 Calculation method

### 3.5.9 Results

For graphic display, the $CO_2$ contour velocity is chosen for the analysis purposes. Other than that, the volume fraction results also retrieved for the pH calculation.

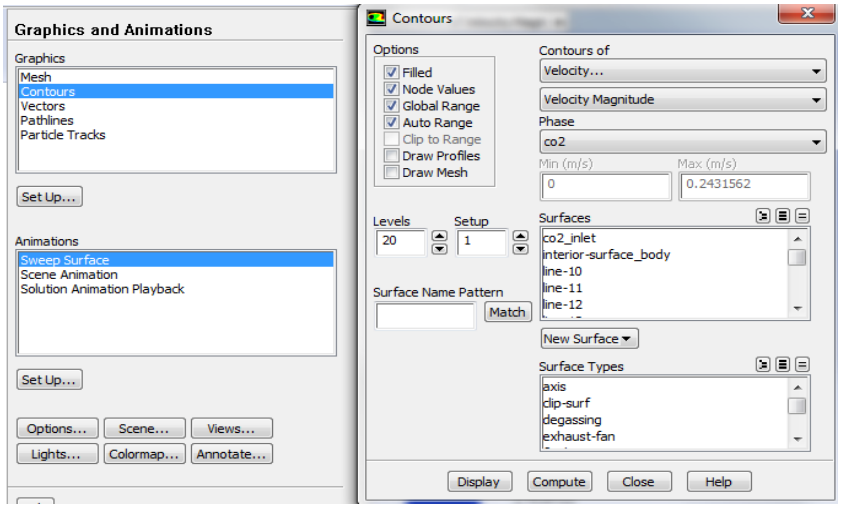


FIGURE 3.25 Graphic and animation setup for post-processing

## 3.6 Gantt Chart and Key Milestone

### 3.6.1 Final Year Project I

TABLE 3.3 Gantt chart and key milestone for FYP1

| | Week | | | | | | | | | | | | | |
|---|---|---|---|---|---|---|---|---|---|---|---|---|---|---|
| Descriptions | 1 | 2 | 3 | 4 | 5 | 6 | 7 | 8 | 9 | 10 | 11 | 12 | 13 | 14 |
| Selection of Project title | | | | | | | | | | | | | | |
| Preliminary research work and literature review | | | | | | | | | | | | | | |
| Submission of extended proposal | | | | | | | | | | | | | | |
| Preparation for proposal defense | | | | | | | | | | | | | | |
| Proposal defense | | | | | | | | | | | | | | |
| Detailed literature review and methodology | | | | | | | | | | | | | | |
| Simulation Work | | | | | | | | | | | | | | |
| Preparation for Interim report | | | | | | | | | | | | | | |
| Submission of Interim report | | | | | | | | | | | | | | |

Gantt Chart

Milestone

### 3.6.2 Final Year Project II

TABLE 3.4 Gantt chart and key milestone for FYP II

| Descriptions | Week | | | | | | | | | | | | | | |
|---|---|---|---|---|---|---|---|---|---|---|---|---|---|---|---|
| | 1 | 2 | 3 | 4 | 5 | 6 | 7 | 8 | 9 | 10 | 11 | 12 | 13 | 14 | 15 |
| Simulation work continue | | | | | | | | | | | | | | | |
| General meeting with supervisor for project presentation | | | | | | | | | | | | | | | |
| Simulation work continue | | | | | | | | | | | | | | | |
| Submission of progress report | | | | | | | | | | | | | | | |
| Compilations of results and finding | | | | | | | | | | | | | | | |
| Poster preparation | | | | | | | | | | | | | | | |
| Pre-sedex | | | | | | | | | | | | | | | |
| Submission of draft report | | | | | | | | | | | | | | | |
| Submission of dissertation | | | | | | | | | | | | | | | |
| Submission of technical paper | | | | | | | | | | | | | | | |
| Viva oral presentation | | | | | | | | | | | | | | | |
| Submission of final dissertation | | | | | | | | | | | | | | | |

Gantt Chart

Milestone

# CHAPTER 4

# RESULTS AND DISCUSSION

Among the results that were predicted from the model, the distribution of bubble size against the depth, to depict the bubble behavior in seawater. Next is to study the bubble velocity with respect to time (s) for two different case studies (variant in depth (m)). This is required to identify the effect bubble dissolution and role of buoyancy on the bubble dynamics as well as its possibility to return to the atmosphere. Other than that, the volume fractions of $CO_2$ against the height where the bubble dissolves in the seawater also were evaluated. This is to check the consequences of $CO_2$ leak into the surrounding water by analyzing the change in seawater pH due to the change in density.

## 4.1 Distribution of bubble size

The distribution of the bubble size in one of the key element to study the effect of $CO_2$ bubble dispersion and dissolution in seawater (Sellami et al., 2015). Based on the distribution size of the bubble, the height travelled (m) by $CO_2$ bubble before it completely dissolve can be observed. Chen at al. (2009) stated that, the bubble plume rise height was more affected by the bubble size rather than the depth. Therefore, it is vital to study the bubble distribution to predict how far the bubble ascends up to the seawater surface before it fully dissolving. The larger the bubble the further it will travel in seawater while smaller bubble will quickly dissolved due to its small diameter.

The distribution sizes of the $CO_2$ bubble after leaked from the seabed are shown in FIGURE 4.1. The distribution of the bubble sizes are reconstructed based on the raw data obtained from QICS experiment as shown in FIGURE 3.1. The.

reconstructions take into account the effect of bubble interactions based on the simulation results. It was found that, almost 50% of the leaked $CO_2$ bubble have diameter varying between 0.0025m (0.25cm) and 0.0050m (0.50cm), 30% with diameter between 0.009m (0.9cm) and 0.010m (1.0cm). While the rest of the bubble resembles as small bubbles (d<0.25cm) and larger bubbles (d>1.0cm) with low presences, both are less than 9%.

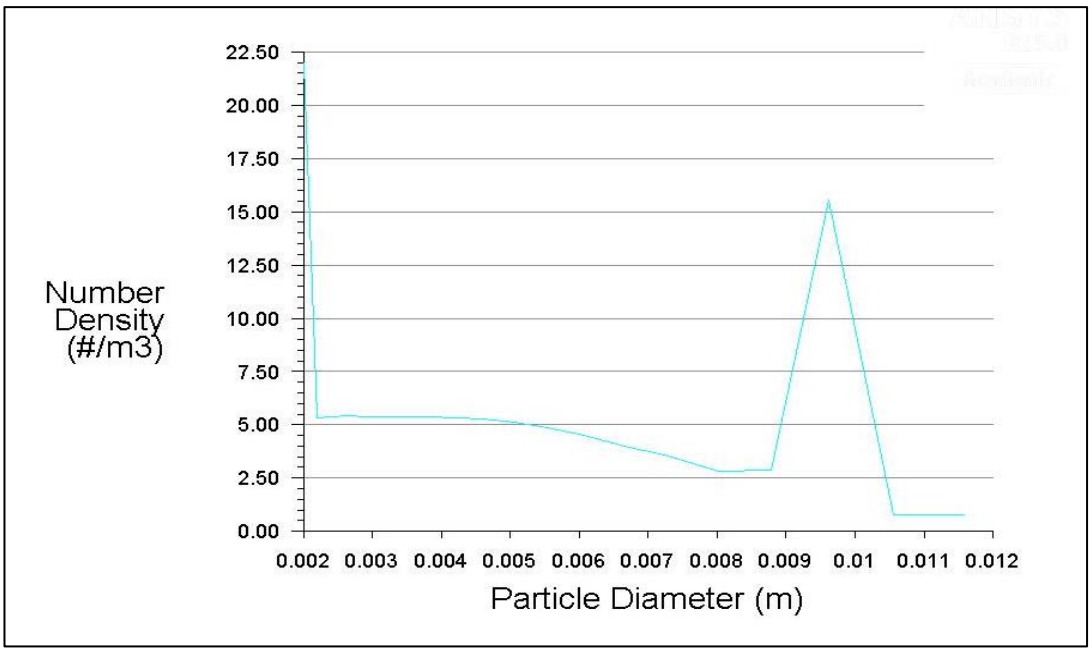


FIGURE 4.1 Size distribution of $CO_2$ bubble in seawater after correlating the effect of bubble interaction

## 4.2 Rising velocity of $CO_2$ bubbles

To examine the rising of $CO_2$ to seawater the model were simulated for 10 minutes after the leak commencing. The $CO_2$ velocity was evaluated at 15 sample points within the computational domain at the leakage distance over 15m taken as the approximate size of the pockmarks.

It was found that, the bubble rises to their terminal height with fast rise velocity (m/s). When the bubble rises up to the sea surface, they tend to grow in size. However, due to its high solubility in seawater, the bubbles quickly shrink to a smaller bubble or dissolve in seawater. According to (Dewar et al., 2015), when a

larger bubble breakup to become a smaller bubble, the rising velocity decreases and consequently dissolve far quicker in seawater. As a result, it will affect the bubble plume structure in seawater. While those with larger diameter, will experience higher velocity and rises up to the surface because of the increase of bubble's buoyant velocity.

The bubble interaction models were incorporated in the modeling which is the Grace et al. Model and Tomiyama lift force model, designated as the drag and lift force respectively. The aim is to study the impact of interaction to the bubble dissolution and behavior.

### 4.2.1 $CO_2$ Velocity contour at Low Tide release (9.5m)

#### i. $CO_2$ velocity contour

(a) 5 minute after leak commencing

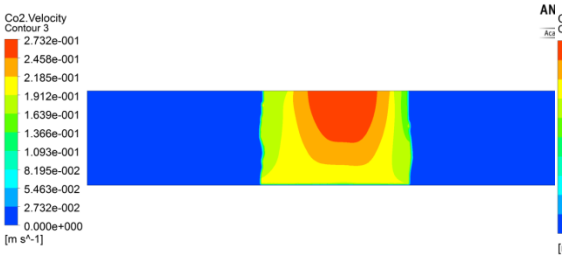


(b) 10 minute after leak commencing

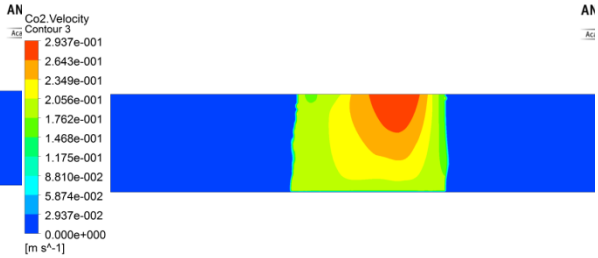


(c) 15 minute after leak commencing


(d) 20 minute after leak commencing

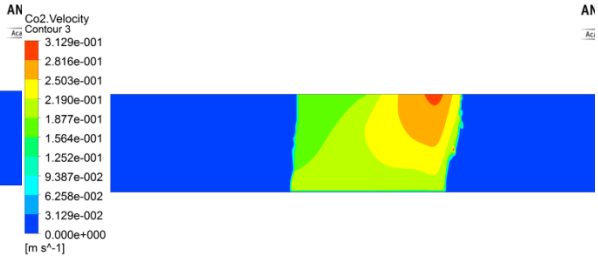


(e) 30 minute after leak commencing


(f) 60 minute after leak commencing


FIGURE 4.2 Velocity contour of $CO_2$ bubble at different time after the leak was commencing for low tide release

The $CO_2$ contour velocity shown in FIGURE 4.2(a) indicates that, within 5 minutes of leak commissioning, the $CO_2$ plume velocity gradually adverted away from the leak point with maximum velocity recorded 0.2732m/s near the sea surface. This also gives indication that most of $CO_2$ bubble already outgassing to the sea surface within short duration of time. The leak was continued to occur for 1 hour and the contour velocity were presented during the 10,15,20,30 and 60 minutes as shown in FIGURE 4.2 (b),(c),(d),(e) and (f) respectively. Overall, the finding shows that the velocity of the $CO_2$ bubbles is higher once it reached the sea surface. This may due to the bubble did not fully dissolve in seawater and exhibit as larger bubble which tend to rise to the sea surface. Meanwhile the velocity of the $CO_2$ bubbles is decreases near the seabed which illustrates the bubble may exist as smaller bubble that dissolves faster in seawater.

### ii. Time for the $CO_2$ bubble to reach the sea surface for low tide scenario

(a) 3 seconds after leak commencing


(b) 5 seconds after leak commencing


(c) 10 seconds after leak commencing


(d) 15 seconds after leak commencing

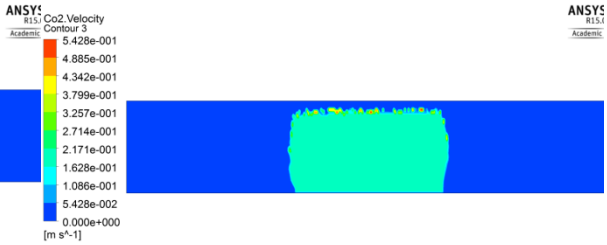


(e) 20 seconds after leak commencing


FIGURE 4.3 Time for the bubble to reach the sea surface at low tide scenario

Based on FIGURE 4.3, the contour shows that the bubbles rise to the terminal height as short as 20 second duration. This is probably due to the shallow depth of the seawater thus caused the bubble to escape to the atmosphere in shorter time. The shallower the depth, the more leaked $CO_2$ bubbles remain unsolved and tend to rise up to the sea surface (atmosphere).

### 4.2.2 $CO_2$ velocity contour at High Tide release (12m)

#### i. $CO_2$ velocity contour

(a) 5 minute after leak commencing

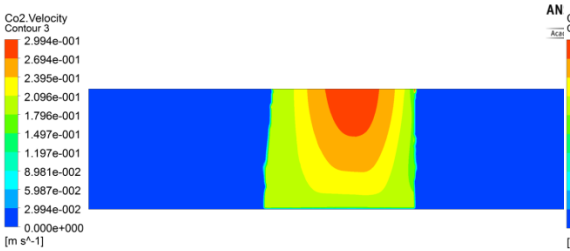


(b) 10 minute after leak commencing

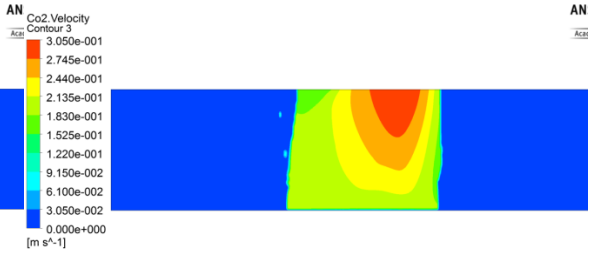


(c) 15 minute after leak commencing

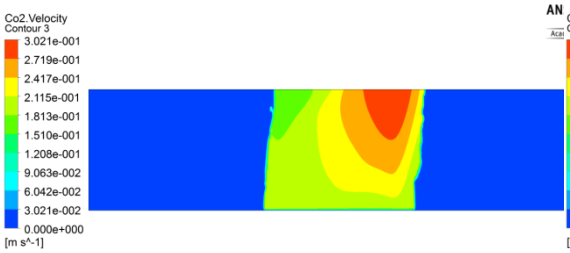


(d) 20 minute after leak commencing

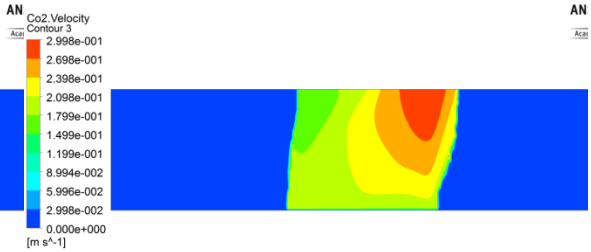


(e) 30 minute after leak commencing

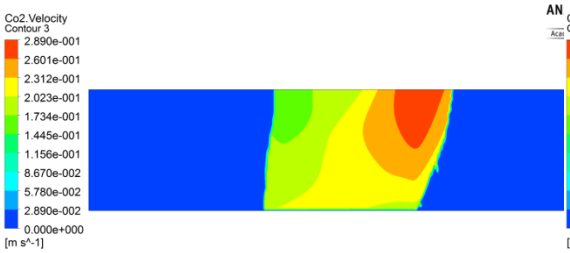


(f) 60 minute after leak commencing


FIGURE 4.4 Velocity contour of $CO_2$ bubble at different time after the leak was commencing for high tide release

Based on FIGURE 4.4(a), the $CO_2$ bubble velocity in high tides shows that the maximum velocity recorded are also near to the sea surface. Upon 5 minutes after the leak was commencing, the maximum velocity of the bubble gives value 0.2994m/s near the sea surface which is slightly higher compare to low tides release. This also depicts that the bubble approaching the sea surface exhibit as larger bubble.

Whereas, the velocity of the bubble is reduces as it closed to the seabed. This configuration tells that the bubble exhibit as smaller bubbles thus reduced its rising velocity to the sea surface due to the higher dissolution rate of $CO_2$ in seawater.

### ii. Time for the $CO_2$ bubble to reach the sea surface for high tide scenario

(a) 3 seconds after leak commencing

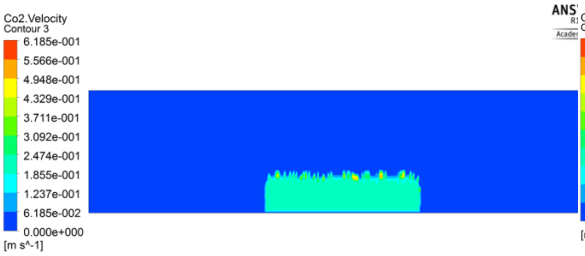


(b) 5 seconds after leak commencing

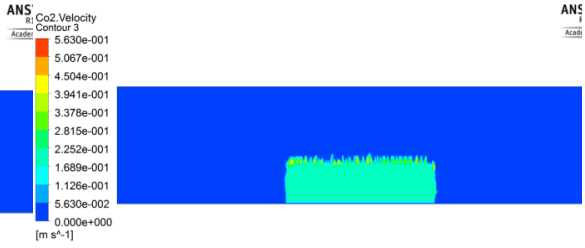


(c) 10 seconds after leak commencing

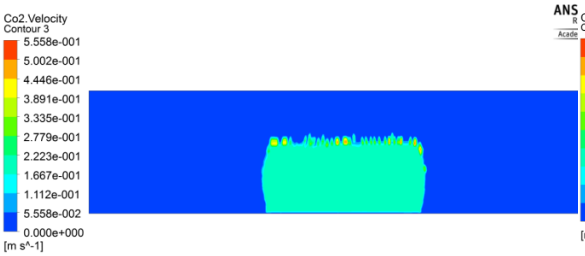


(d) 15 seconds after leak commencing


(e) 20 seconds after leak commencing

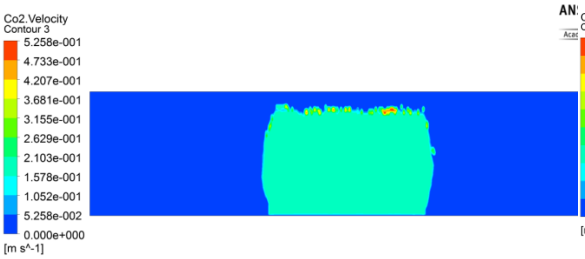


(f) 25 seconds after leak commencing


(g) 30 seconds after leak commencing


FIGURE 4.5 Time for the bubble to reach the sea surface for high tide scenario

Based on FIGURE 4.5, the contour shows that the minimum time for the bubbles to rise to the terminal height for high tide release surface is 30 seconds compare to low tides release with 20 seconds duration for the bubble to reach the sea

surface. This may due to the higher depth of the seawater thus reduces the time taken for the bubble to escape to the atmosphere. However, there is still probability that the bubble rises up to the sea surface.

The key elements which need to be evaluate further, is the dangers of; the larger bubble rising beyond the sea surface especially at a shallow depth or the smaller bubbles that dissolves quickly and possibly giving large pH change in seawater.

### 4.3 pH Change in seawater

When $CO_2$ dissolve in the seawater, it will undergo chemical reaction to form carbonic acid resulting to the increase of local seawater acidity. A small scale modeling to study the impact of $CO_2$ leaked from sub-seabed or pipeline within the North Sea and the surrounding water done by (Dewar et al., 2013a) shows the variability of pH change from dissolved $CO_2$ solution. Their study shows that the seasonal data affects the change in pH due to the change in the density.

The change in pH of the seawater can be estimated by analyzing the generation of positive hydrogen ions $[H^+]$ that results in decrease of pH and caused the ocean to become more acidic (IPCC, 2005). Hoffert et al. (1979) provide methods to calculate the pH. When the $CO_2$ dissolved in seawater, it will dissociates into bicarbonate $[HCO_3^-]$ ion and $[H^+]$ ions and further separated into carbonate $[CO_3^{2-}]$ ions and $[H^+]$ (Dissanayake et al., 2012). The number of ions is dependent on the concentration of the dissolve $CO_2$ (Dewar et al., 2013a). The calculation for total carbon dioxide concentration (mol/L or M) can be defined as the following;

$$\sum CO_2 = \left(\frac{[H^+]}{[H^+]+2K_2}\right) \times \left(1 + \frac{k_2}{[H^+]}\frac{[H^+]}{k_1}\right) \times \left([H^+] - \frac{k_w}{H^+}\right) \quad (41)$$

The concentration of $CO_2$ in seawater is expressed as function of volume fraction and can be calculated using the following formula;

$$[CO_2] = \frac{\rho}{M} \times V_f \quad (42)$$

Where ρ is density of $CO_2$ in g/L, M is molar mass in g/mole and $V_f$ is the volume fraction.

According to Dissanayake et al. (2012) thermal equilibrium constant ($k_{i=1,2}$)for the dissociation of carbonic acid are given as;

$$k_1 = \frac{[HCO_3^-][H^+]}{CO_2} \tag{43}$$

$$k_2 = \frac{[CO_3^{2-}][H^+]}{[HCO_3^-]} \tag{44}$$

The value of $k_1$ and $k_2$ can be obtained from equations introduced by Saruhashi (1970). The values are calculated using function of pressure and temperature as shown below;

$$pk_1 = \frac{3416.6675}{T} + 0.032902T - 14.9179 \tag{45}$$

$$pk_2 = \frac{2902.39}{T} + 0.02379T - 6.4980 \tag{46}$$

Meanwhile, the ion content ($k_w$) of the water can be obtained from equation below using data from Marshall and Frank (1981) as suggested by Someya et al. (2005) (Dewar et al., 2013b).

$$k_{w(0.1MPa)} = 3.7853T^3 \times 10^{-19} - 3.1197T^2 \times 10^{-16} + 8.5871T \times 10^{-14} - 7.8923 \times 10^{-12} \tag{47}$$

$$k_{w(P)}/k_{w(0.1MPa)} = 1.0006171 + 9.0589 \times 10^{-3}p + 4.4532 \times 10^{-5}p^2 \tag{48}$$

Solve all equations above to obtain the value of $[H^+]$. Then the pH calculation was presented through negative logarithm of the ion content (Dewar et al., 2013b).

$$pH = -\log_{10}[H^+] \tag{49}$$

The baseline pH of the seawater is taken as 8.05-8.10 pH from the QICS experiment (Shitashima et al., 2015; Dewar et al., 2015). The pH was measured at 3cm above the seabed considering the location of real time sensor applied in the in situ sensor for QICS experiment carried out by Shitashima et al. (2015). The pH calculation is carried out at 15 sample points along (x-direction) the leakage area.

The individual pressure of the sample point is used to calculate value of $k_1$, $k_2$, and $k_w$ as shown in TABLE 4.3 and TABLE 4.4 at APPENDIX 3. The volume fractions of $CO_2$ were used to calculate the $CO_2$ concentrations thus give corresponding value of $[H^+]$ to measure the change in pH of the seawater.

### 4.3.1 pH change for low tide scenario

TABLE 4.1 Change in pH due to change in volume fraction for low tide release scenario

| Sample | Volume fraction | [H+] | ΔpH |
|---|---|---|---|
| 1 | 0.752 | 1.60639535 | -0.205852438 |
| 2 | 0.752 | 1.60639535 | -0.205852438 |
| 3 | 0.752 | 1.60639535 | -0.205852438 |
| 4 | 0.759 | 1.613884242 | -0.207872381 |
| 5 | 0.760 | 1.61494334 | -0.20815729 |
| 6 | 0.761 | 1.616001731 | -0.208441822 |
| 7 | 0.762 | 1.617067366 | -0.208728113 |
| 8 | 0.761 | 1.616001731 | -0.208441822 |
| 9 | 0.761 | 1.616001731 | -0.208441822 |
| 10 | 0.760 | 1.61494334 | -0.20815729 |
| 11 | 0.759 | 1.613884242 | -0.207872381 |
| 12 | 0.759 | 1.613884242 | -0.207872381 |
| 13 | 0.759 | 1.613884242 | -0.207872381 |
| 14 | 0.752 | 1.60639535 | -0.205852438 |
| 15 | 0.752 | 1.60639535 | -0.205852438 |

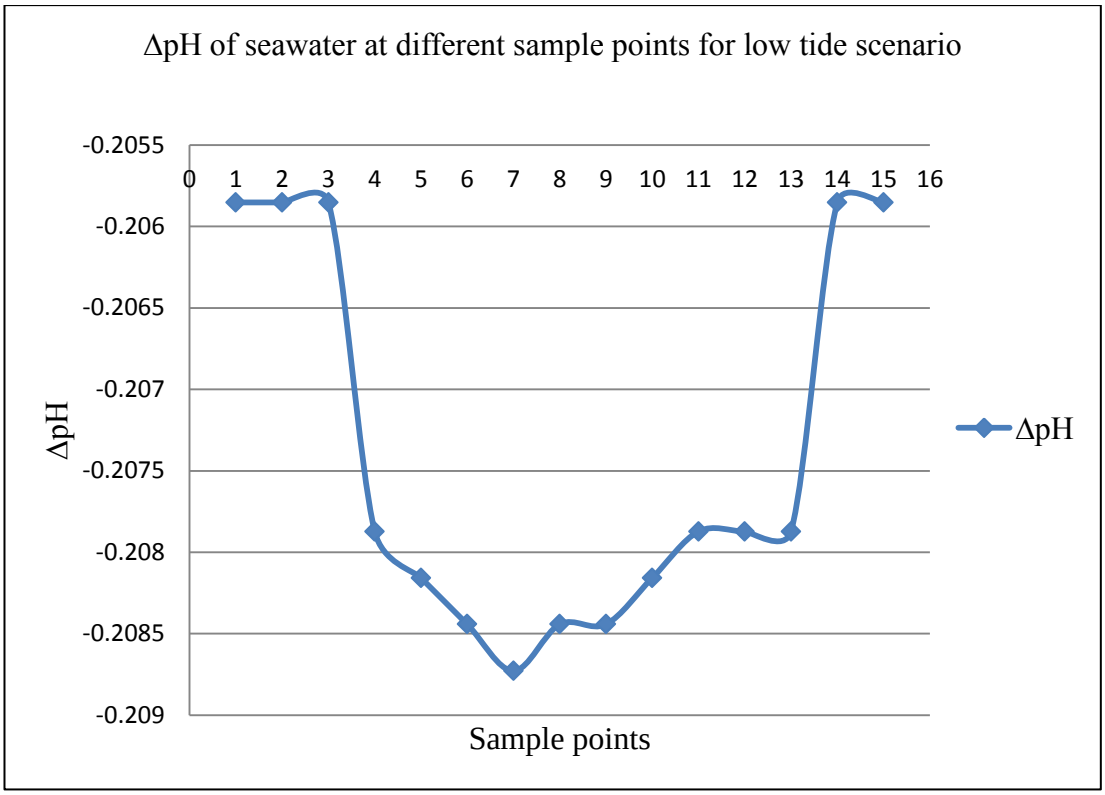


FIGURE 4.6 ΔpH of seawater at different sample points for low tide scenario

### 4.3.2 pH change for high tide scenario

TABLE 4.2 Change in pH due to change in volume fraction for high tide release scenario

| Sample | Volume fraction | [H+] | ΔpH |
|---|---|---|---|
| 1 | 0.780 | 1.636128609 | -0.213817439 |
| 2 | 0.780 | 1.636128609 | -0.213817439 |
| 3 | 0.789 | 1.645578868 | -0.216318702 |
| 4 | 0.790 | 1.64663368 | -0.216596994 |
| 5 | 0.790 | 1.64663368 | -0.216596994 |
| 6 | 0.791 | 1.647687844 | -0.216874938 |
| 7 | 0.791 | 1.647687844 | -0.216874938 |
| 8 | 0.792 | 1.648741363 | -0.217152534 |
| 9 | 0.792 | 1.648741363 | -0.217152534 |
| 10 | 0.791 | 1.647687844 | -0.216874938 |
| 11 | 0.790 | 1.64663368 | -0.216596994 |
| 12 | 0.790 | 1.64663368 | -0.216596994 |
| 13 | 0.789 | 1.645578868 | -0.216318702 |
| 14 | 0.789 | 1.645578868 | -0.216318702 |
| 15 | 0.780 | 1.636128609 | -0.213817439 |

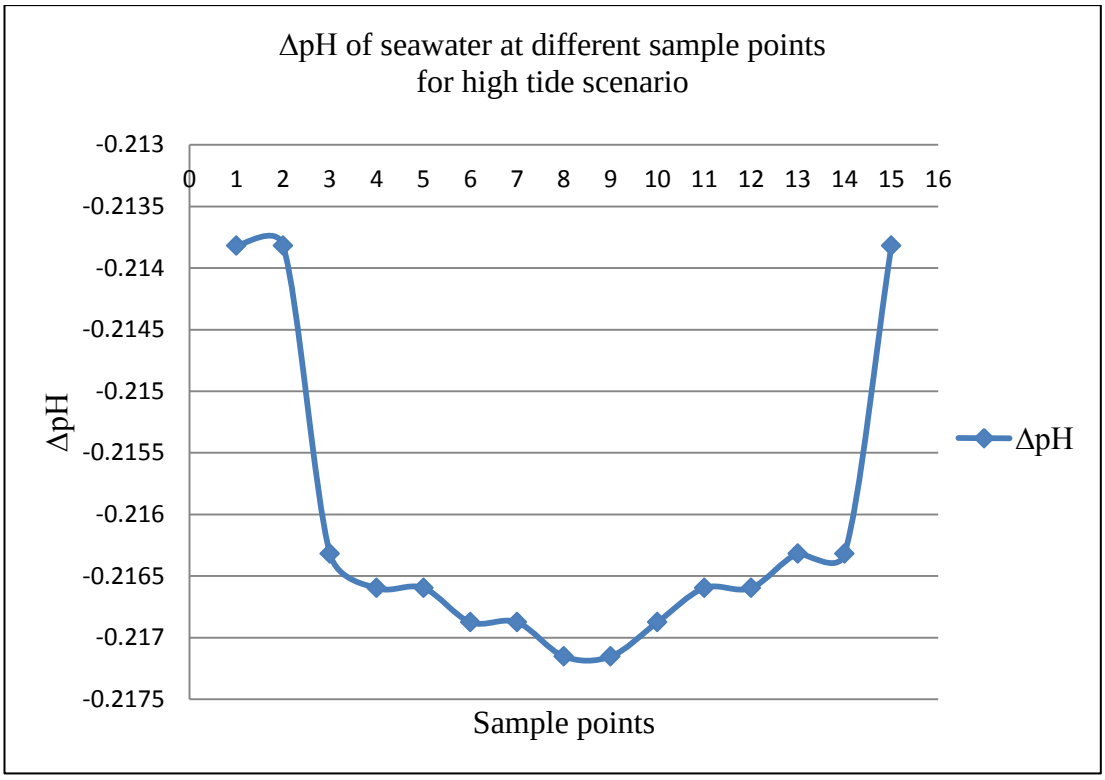


FIGURE 4.7 ΔpH of seawater at different sample points for high tide scenario

Based on FIGURE 4.6 and FIGURE 4.7, the ΔpH values decrease as the volume fraction of CO2 increase. The trend shows that, for both release scenarios major decrease of pH is found within the area of the CO2 leakage points; sample point 6 to 9 and sample points 6 to 10 for low tide scenario and high tide scenario respectively. However, these pH values are taken based on volume fraction of CO2 at the individual sample points only. The parameters which need to be evaluated further are the danger of CO2 bubble plumes in which the total concentration of the plume could increase the change in pH even more compare to individual sample.

Other than that, the bubble plume rise height also provides significant impact to the pH change. For low tide release, the maximum volume fraction of $CO_2$ measured at 3cm is 0.762, while 0.792 is recorded for high tide scenario. The pH decreases (ΔpH: -0.2059 to -0.2087) observed in low tide scenario and (ΔpH: -0.2138 to -0.2172) recorded for high tide scenario. The significant changes in pH value are then used to predict the consequence of $CO_2$ bubble leakage in seawater and describe the effect to the marine environment.

## 4.4 Model validation

### 4.4.1 Velocity distribution of $CO_2$ bubble

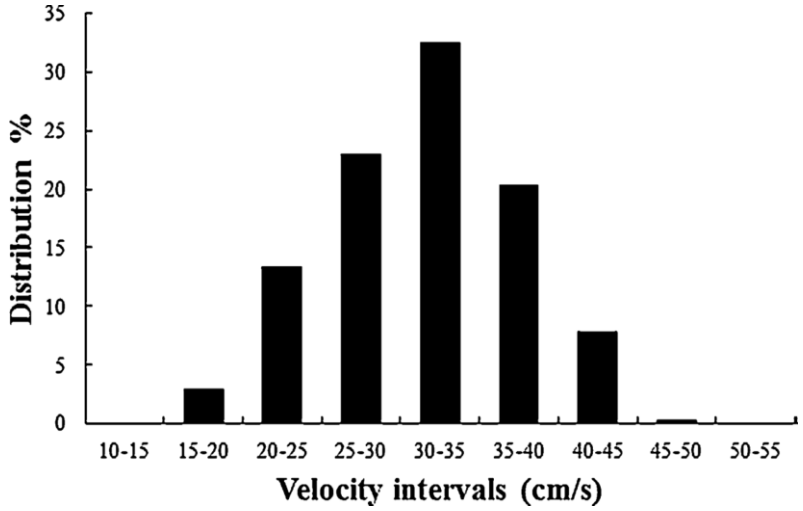


FIGURE 4.8 Velocity distribution of $CO_2$ bubble obtained from QICS experimental data (Sellami et al., 2015).

FIGURE 4.8 illustrates the observable $CO_2$ bubble velocity obtained from the QICS experiment. Based on the figure, most of the bubble (>75%) velocity ranging between 25cm/s and 40cm/s (Sellami et al., 2015). Based on the finding shows in FIGURE 4.2 and FIGURE 4.4; for low tide leak, the bubbles (>50%) rise with velocity ranging between 0.172m/s (17.2cm/s) and 0.315m/s (31.5cm/s). While, for high tide leak, most of the bubble (>50%) have velocity ranging between 0.173m/s (17.3cm/2) and 0.305m/s (30.5cm/s).

As compared to the experimental data, the simulation results illustrates deviation in bubble velocity around 25% and 26% for low tide leak and high tide leak respectively. This may influenced by the distribution of the size of particle as shown in FIGURE 4.1, as the reconstruction of the size interval is done automatically using discrete function in the ANSYS Fluent software thus affecting the bubble interactions as well as its velocity.

The finding also shows that, more bubble exhibit as larger bubble caused the dissolution become more distributed in addition of interaction factor thus reduced its

dissolution rate. In contrast, smaller bubbles provide larger interfacial area between the bubble and seawater which increase the dissolution rates.

This model has confirmed the finding done by Dewar et al. (2013b), with large number of smaller bubbles, the plume height the $CO_2$ bubbles travelled and the velocity are reduces because of the enhancement of $CO_2$ dissolution rate. While, larger bubbles could mitigate to the water surface much faster. Overall, the simulation results match the outcome observed from the experiment, where some bubbles are found to reach the sea surface for shallow leak scenario (Dewar et al., 2015).

### 4.4.2 Impact of leaked $CO_2$ in seawater

The change in $CO_2$ concentration with given change in volume fraction, in addition to the maximum change in pH can be used to predict the consequences of $CO_2$ leakage in seawater. Study done by Shitashima et al. (2015) shows decrease in pH (ΔpH: -1.5 to -2.2pH) for measured $CO_2$ release above the seafloor. As seen from FIGURE 4.6 and FIGURE 4.7, the maximum pH reductions are ΔpH: -0.2087 and ΔpH: -0.2172 observed for low and high tide scenario respectively measured at depth of 3cm occur directly above leakage area. These results depict that, the pH change is not significant if measured only through the sample points. The impact to the marine organisms is likely if the $CO_2$ continuously leak at the same location with high dissolution rate, created large bubble plume thus causing high change in pH. Yet, the data of individual volume fractions at different sample points that were used to estimate the $CO_2$ concentration was not enough to perform the analysis to study the impact of change in seawater pH. The overall concentration change of seawater instead should be used to estimate the change in pH.

Other than that, the factor that result low change in pH obtained from the simulation due to more $CO_2$ bubble ascends up to the sea surface within shorter time. This inhibits the dissolution of $CO_2$ to seawater thus reduced its concentration. Hence, the calculated change in pH seen as not significant especially for shallow leakage scenario as most of the bubbles are dispersed to the atmosphere. Moreover,

the field data from QICS experiment is necessary to perform the simulation to obtain more accurate results.

Compared to QICS experiment conditions, the real scenario for sub-seabed CCS would be deeper for example the Sleipner site around 100m depth (Shitashima et al., 2015). The potential escape of $CO_2$ to sea-surface should be evaluated further in deeper depth as the rising velocity of $CO_2$ would be different as in shallow depth. High change in pH is expected for deep leakage scenario because more bubble will dissolve in seawater due to eruption of bubble as results of tidal oscillation.

# CHAPTER 5

# CONCLUSION AND RECOMMENDATION

## 5.1 Conclusion

Managing consequences of $CO_2$ leakage is very challenging. A comprehensive appreciation of risk must consider the likelihood that leakage will happen and the potential recovery of organisms and ecosystems once the leak has ceased (Stephen et al., 2013). It is well understood that the development of CCS technology achieve acceptance if the prediction of the consequences of different mode of the plant and infrastructure failure is well established (Zhang & Chen, 2010). However, the study $CO_2$ leakage is still within research and developments phase especially the release of $CO_2$ under the sea and their impact to marine environment.

In this study, a computational fluid dynamics approach were used to evaluate the consequences of $CO_2$ bubble dissolution in seawater based on two scenario for $CO_2$ leakage at low and high tides. The results obtained from study done by Dewar et al. (2015) were used for model validation. The distribution of bubble size leaked from the sediment that was obtained from QICS experiment varying between 0.002m and 0.012m which observed based on the pockmark location. Reconstructions of the size distribution were done through the application of discrete method in the population balance model.

To investigate the fate of bubble dissolution in seawater, the behavior of rising of bubbles plume to the sea surface were evaluated through the rising velocity of $CO_2$ within the computational domain. It was found that, for both low and high tides scenario the larger bubble rises up to the sea surface (atmosphere) while,

smaller bubble will dissolve faster in seawater and the maximum $CO_2$ velocity was recorded at the sea surface.

The changes on pH water were studied to measure the impact of the leak $CO_2$ to the surrounding water especially to the marine organism. For this case, the volume fractions are used to calculate the total concentration of $CO_2$. The change in pH measured 3cm above the seafloor shows maximum decrease in pH of ΔpH: -0.2087 and ΔpH: -0.2172 observed for low and high tide scenario respectively. The slight change in pH illustrate that low dissolution rate of $CO_2$ in seawater for the release scenario as more bubble has escalated to the sea surface.

## 5.2 Recommendation

To obtained more prove useful results, the field data from QICS experiment or other future small scale lab experiment and in-situ experiment are required to model the $CO_2$ leakage scenario in seawater. This is vital for the determination of true value in predicting the effect of the leak to the surrounding water and for verification of model's viability (Dewar et al., 2013b). More detailed data can improve the quality of the simulation. On the other hand, simulation may be carried out longer than 60 minutes to study the impact of long term $CO_2$ release.

Other than that, this model was modeled using the standard k-$\varepsilon$ model. As the strength and weaknesses of the standard k-$\varepsilon$ model have become known, modifications were done for improvement. Therefore, for future work the RNG k-$\varepsilon$ model or realizable k-$\varepsilon$ model may be used for the simulation work to improve the results.

According to Adams et al. (1993), for larger leakage rate of CO2 in deep ocean, the $CO_2$ concentration would be higher because of high solubility of $CO_2$ into the water (Dewar et al., 2015). Therefore, deep release scenario is suggested for future simulation work to study the impact of pH change of seawater as the dissolution of the $CO_2$ bubble is predicted to be more vigorous in deeper depth ocean compared to shallow depth scenario.

# REFERENCES


ANSYS. (2013). ANSYS Fluent Theory Guide.

Artioli, Y., Blackford, J.C., Butenschon, M., Holt, J.T., Wakeline, S.L., Thomas, H., Borges, A.V., & Allen, J.I. (2012). The carbonate system in the North Sea: Sensitivity and model validation. *Journal of Marine system*, 102-104.

Bai, Y., & Bai, Q. (2014). Chapter 8 - Risk Analysis for Subsea Pipelines. In Y. B. Bai (Ed.), *Subsea Pipeline Integrity and Risk Management* (pp. 169-212). Boston: Gulf Professional Publishing.

Beaubien, S. E., De Vittor, C., McGinnis, D. F., Bigi, S., Comici, C., Ingrosso, G., . . . Ruggiero, L. (2014). Preliminary Experiments and Modelling of the Fate of CO2 Bubbles in the Water Column Near Panarea Island (Italy). *Energy Procedia*, *59*(0), 397-403.

Blackford, J., Bull, J. M., Cevatoglu, M., Connelly, D., Hauton, C., James, R. H., . . . Wright, I. C. (2015). Marine baseline and monitoring strategies for carbon dioxide capture and storage (CCS). *International Journal of Greenhouse Gas Control*, *38*(0), 221-229. doi: http://dx.doi.org/10.1016/j.ijggc.2014.10.004

Blackford, J., Hattam, C., Widdicombe, S., Burnside, N., Naylor, M., Kirk, K., . . . Wright, I. (2013). 7 - CO2 leakage from geological storage facilities: environmental, societal and economic impacts, monitoring and research strategies. In J. Gluyas & S. Mathias (Eds.), *Geological Storage of Carbon Dioxide (co2)* (pp. 149-178): Woodhead Publishing.

Blackford, J. C., Torres, R., Cazanave, P., & Artioli, Y. (2013). Modelling Dispersion of CO2 Plumes in Sea Water as an Aid to Monitoring and Understanding Ecological Impact. *Energy Procedia*, *37*(0), 3379-3386. doi: http://dx.doi.org/10.1016/j.egypro.2013.06.226

Cai, W.J., Bauer, J.E., Raymond, P.A., Bianchi, T.S., Hopkinson, C.S., & Regnier, P.A.G. (2013). The changing carbon cycle of the coastal ocean. *Nature, 504*, 61-70. doi: 10.1038/nature12857

Caramanna, G., Andre', N., Dikova, M. P., Rennie, C., & Maroto-Valer, M. M. (2014). Laboratory experiments for the assessment of the physical and chemical impact of potential CO2 seepage on seawater and freshwater environments. *Energy Procedia*, *63*(0), 3138-3148.

Chen, B., Nishio, M., Song, Y., & Akai, M. (2009). The fate of CO2 bubble leaked from seabed. *Energy Procedia, 1*(1), 4969-4976.

Dewar, M., Sellami, N., & Chen, B. (2015). Dynamics of rising CO2 bubble plumes in the QICS field experiment: Part 2 – Modelling. *International Journal of Greenhouse Gas Control, 38*(0), 52-63.

Dewar, M., Wei, W., McNeil, D., & Chen, B. (2013a). Simulation of the Near Field Physiochemical Impact of CO2 Leakage into Shallow Water in the North Sea. *Energy Procedia, 37*, 3413-3423.

Dewar, M., Wei, W., McNeil, D., & Chen, B. (2013b). Small-scale modelling of the physiochemical impacts of CO2 leaked from sub-seabed reservoirs or pipelines within the North Sea and surrounding waters. *Marine Pollution Bulletin, 73*(2), 504-515.

Dickson, A.G., Sabine, C.L., & Christian, J.R.(2007). Guide to best practice for ocean CO2 measurement. *PICES Special Publication,3*(0), 191.

Dissanayake, A. L., DeGraff, J. A., Yapa, P. D., Nakata, K., Ishihara, Y., & Yabe, I. (2012). Modeling the impact of CO2 releases in Kagoshima Bay, Japan. *Journal of Hydro-environment Research, 6*(3), 195-208.

Gibbins, J., & Chalmers, H. (2008). Carbon capture and storage. *Energy Policy, 36*(12), 4317-4322. doi: http://dx.doi.org/10.1016/j.enpol.2008.09.058

Global CCS Institute. (2013). Hazard analysis for offshore carbon capture platforms and offshore pipeline.

Han, J.-H., Ahn,Y.-C., Lee,J.-U., & Lee',I.-B. (2012). Optimal strategy for carbon capture and storage infrastructure : A review. *Korean J. Chem. Eng. 29* (8), 975-984.

Harper, P., Wilday, J.,& Bilio,M.(2011). Assessment of the major hazard potential of carbon dioxide ($CO_2$). Health and Safety Executive. Retrieved October 31, 2015 from http://www.hse.gov.uk/carboncapture/assets/docs/major-hazard-potential-carbon-dioxide.pdf

Ha-Duong, M., & Loisel, R. (2011). Actuarial risk assessment of expected fatalities attributable to carbon capture and storage in 2050. *International Journal of Greenhouse Gas Control, 5*(5), 1346-1358.

Herzog, N., & Egbers, C. (2013). Atmospheric Dispersion of CO2 Released from Pipeline Leakages. *Energy Procedia, 40*(0), 232-239.

Hill, T. A., Fackrell, J. E., Dubal, M. R., & Stiff, S. M. (2011). Understanding the consequences of CO2 leakage downstream of the capture plant. *Energy Procedia, 4*(0), 2230-2237.

Hvidevold, H. K., Alendal, G., Johannessen, T., & Mannseth, T. (2012). Assessing model parameter uncertainties for rising velocity of CO2 droplets through experimental design. *International Journal of Greenhouse Gas Control, 11*(0), 283-289. doi: http://dx.doi.org/10.1016/j.ijggc.2012.09.008

International Energy Agency (IEA).(2015). Energy and climate change. World energy outlook special report. Retrieved October 20, 2015 from https://www.iea.org/publications/freepublications/publication/WEO2015SpecialReportonEnergyandClimateChange.pdf

Intergovernmental Panel on Climate Change (IPCC).(2005).Carbon Capture and Storage. *Cambridge University Press, New York,1* (0).

Jones, D. G., Beaubien, S. E., Blackford, J. C., Foekema, E. M., Lions, J., De Vittor, C., . . . Queirós, A. M. (2015). Developments since 2005 in understanding potential environmental impacts of CO2 leakage from geological storage. *International Journal of Greenhouse Gas Control*(0).

Luo, Y. W., Doney, S. C., Anderson, L. A., Benavides, M., Bode, A., Bonnet, S., . . . Zehr, J. P. (2012). Database of diazotrophs in global ocean: abundances, biomass and nitrogen fixation rates. *Earth Syst. Sci. Data Discuss., 5*(1), 47-106. doi: 10.5194/essdd-5-47-2012

Kano, Y., Sato, T., Kita, J., Hirabayashi, S., & Tabeta, S. (2010). Multi-scale modeling of CO2 dispersion leaked from seafloor off the Japanese coast. *Marine Pollution Bulletin, 60*(2), 215-224.

King Abdullah Petroleum Studies and Research Centre (KAPSARC).(2012). Carbon Capture and Storage: Technologies, Policies, Economics and Implementation Strategies. *CRC Press*.

Kita, J., Stahl, H., Hayashi, M., Green, T., Watanabe, Y., & Widdicombe, S. (2015). Benthic megafauna and CO2 bubble dynamics observed by underwater photography during a controlled sub-seabed release of CO2. *International Journal of Greenhouse Gas Control, 38*(0), 202-209.

Phelps, J. J. C., Blackford, J. C., Holt, J. T., & Polton, J. A. (2015). Modelling large-scale CO2 leakages in the North Sea. *International Journal of Greenhouse Gas Control, 38*(0), 210-220.

Sellami, N., Dewar, M., Stahl, H., & Chen, B. (2015). Dynamics of rising CO2 bubble plumes in the QICS field experiment: Part 1 – The experiment. *International Journal of Greenhouse Gas Control, 38*(0), 44-51.

Shitashima, K., Maeda, Y., & Ohsumi, T. (2013). Development of detection and monitoring techniques of CO2 leakage from seafloor in sub-seabed CO2 storage. *Applied Geochemistry, 30*(0), 114-124.

Shitashima, K., Maeda, Y., & Sakamoto, A. (2015). Detection and monitoring of leaked CO2 through sediment, water column and atmosphere in a sub-seabed CCS experiment. *International Journal of Greenhouse Gas Control, 38*. doi: http://dx.doi.org/10.1016/j.ijggc.2014.12.011

Someya, S., Bando, S., Song, Y., Chen, B.,& Nishio, M. (2005). DeLIF measurement of PH distribution around dissolving CO2 droplet in high pressure vessel. *International Journal of Heat and Mass Transfer, 48(12)*, 2508-2515. doi: http://dx.doi.org/10.1016/j.ijheatmasstransfer.2004.12.042

Taylor, P., Stahl, H., Vardy, M. E., Bull, J. M., Akhurst, M., Hauton, C., . . . Blackford, J. (2015). A novel sub-seabed CO2 release experiment informing monitoring and impact assessment for geological carbon storage. *International Journal of Greenhouse Gas Control, 38*(0), 3-17. doi: http://dx.doi.org/10.1016/j.ijggc.2014.09.007

Uilhoorn, F. E. (2013). Evaluating the risk of hydrate formation in CO2 pipelines under transient operation. *International Journal of Greenhouse Gas Control, 14*(0), 177-182. doi: http://dx.doi.org/10.1016/j.ijggc.2013.01.021

Wang, H., & Duncan, I. J. (2014). Likelihood, causes, and consequences of focused leakage and rupture of U.S. natural gas transmission pipelines. *Journal of Loss Prevention in the Process Industries, 30*(0), 177-187. doi: http://dx.doi.org/10.1016/j.jlp.2014.05.009

Wennersten, R., Sun, Q., & Li, H. (2015). The future potential for Carbon Capture and Storage in climate change mitigation – an overview from perspectives of technology, economy and risk. *Journal of Cleaner Production, 103*(0), 724-736. doi: http://dx.doi.org/10.1016/j.jclepro.2014.09.023

Widdicombe, S., McNeill, C. L., Stahl, H., Taylor, P., Queirós, A. M., Nunes, J., & Tait, K. (2015). Impact of sub-seabed CO2 leakage on macrobenthic community structure and diversity. *International Journal of Greenhouse Gas Control, 38*(0), 182-192. doi: http://dx.doi.org/10.1016/j.ijggc.2015.01.003

Yang, N., & Wang, R. (2015). Sustainable technologies for the reclamation of greenhouse gas CO2. *Journal of Cleaner Production, 103*(0), 784-792. doi: http://dx.doi.org/10.1016/j.jclepro.2014.10.025

Zhang, B., & Chen, G.-m. (2010). Quantitative risk analysis of toxic gas release caused poisoning—A CFD and dose–response model combined approach. *Process Safety and Environmental Protection, 88*(4), 253-262. doi: http://dx.doi.org/10.1016/j.psep.2010.03.003

# APPENDICES

APPENDIX 1

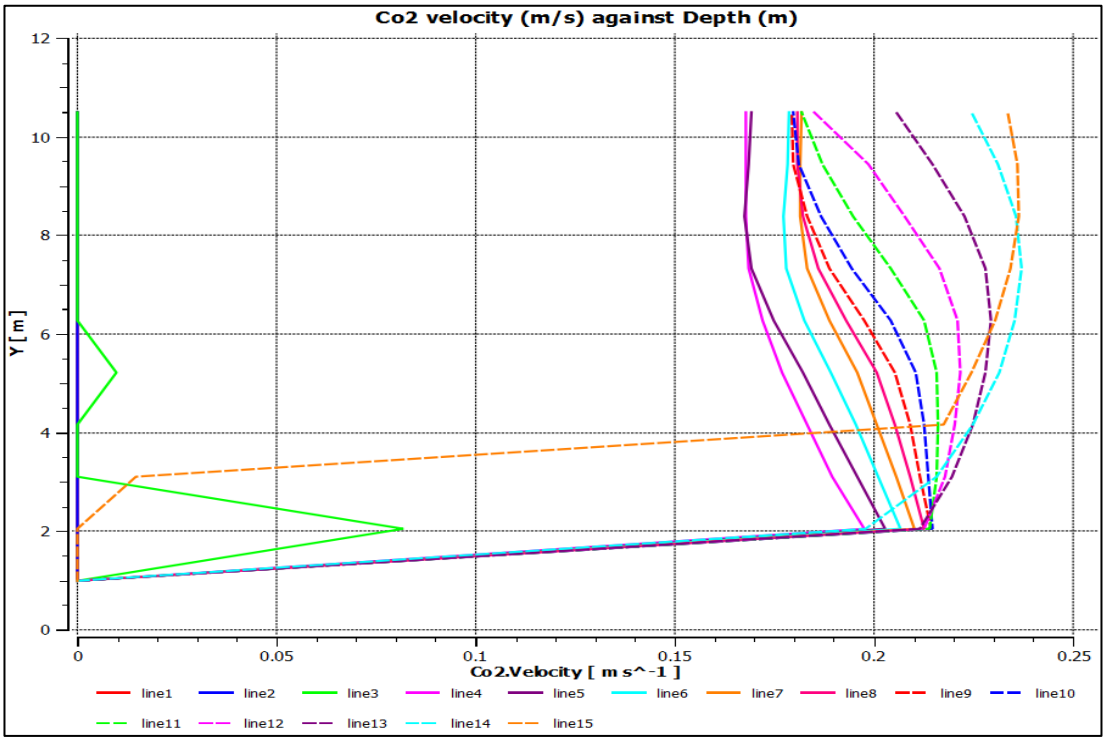


FIGURE 4.9 $CO_2$ velocity (m/s) against depth (m) for low tide release

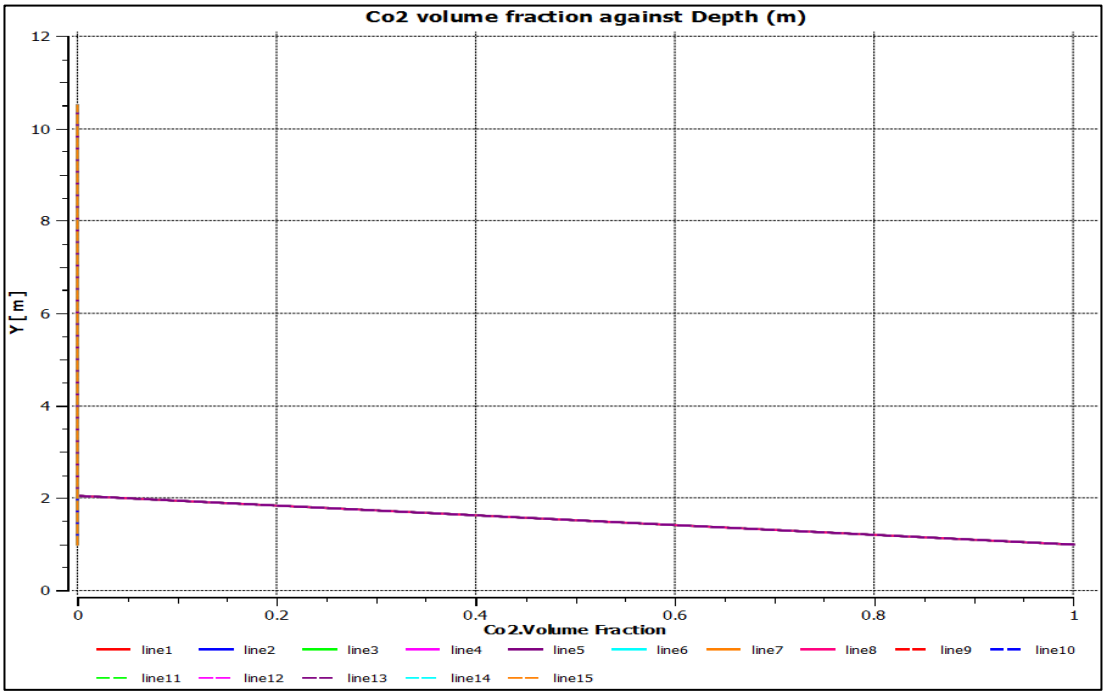


FIGURE 4.10 $CO_2$ volume fraction against depth (m) for low tide release

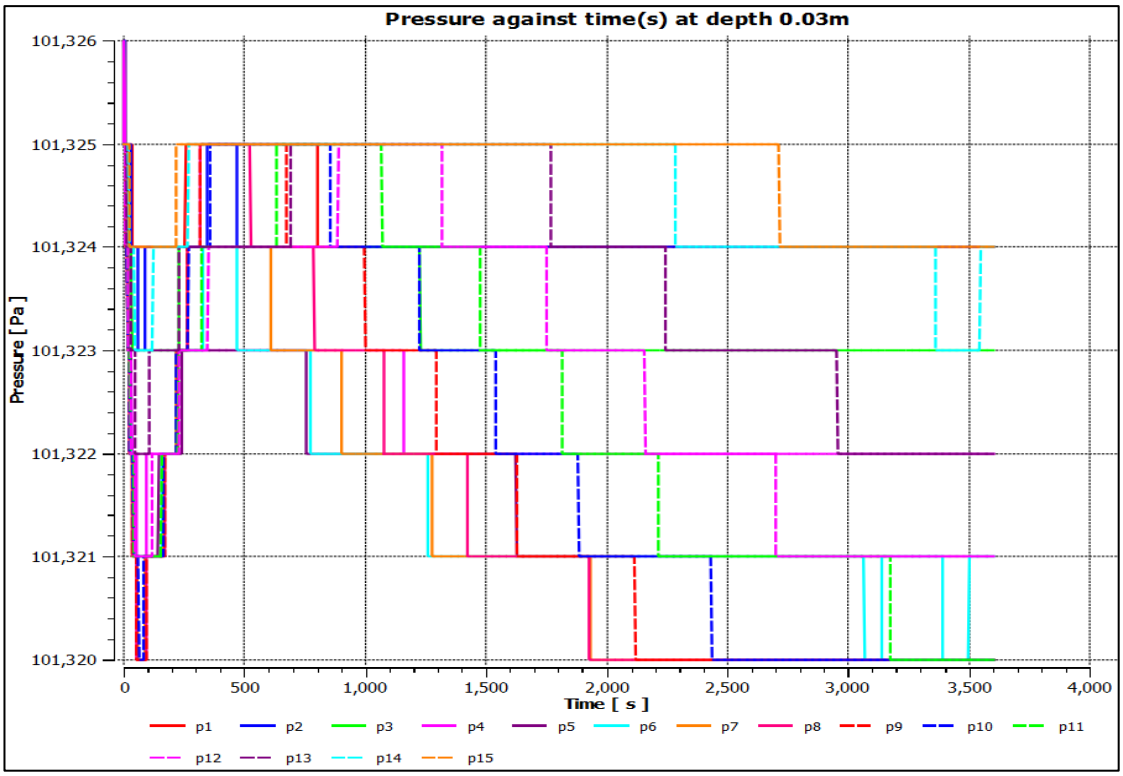


FIGURE 4.11 Pressure measured at depth 3cm

APPENDIX 2

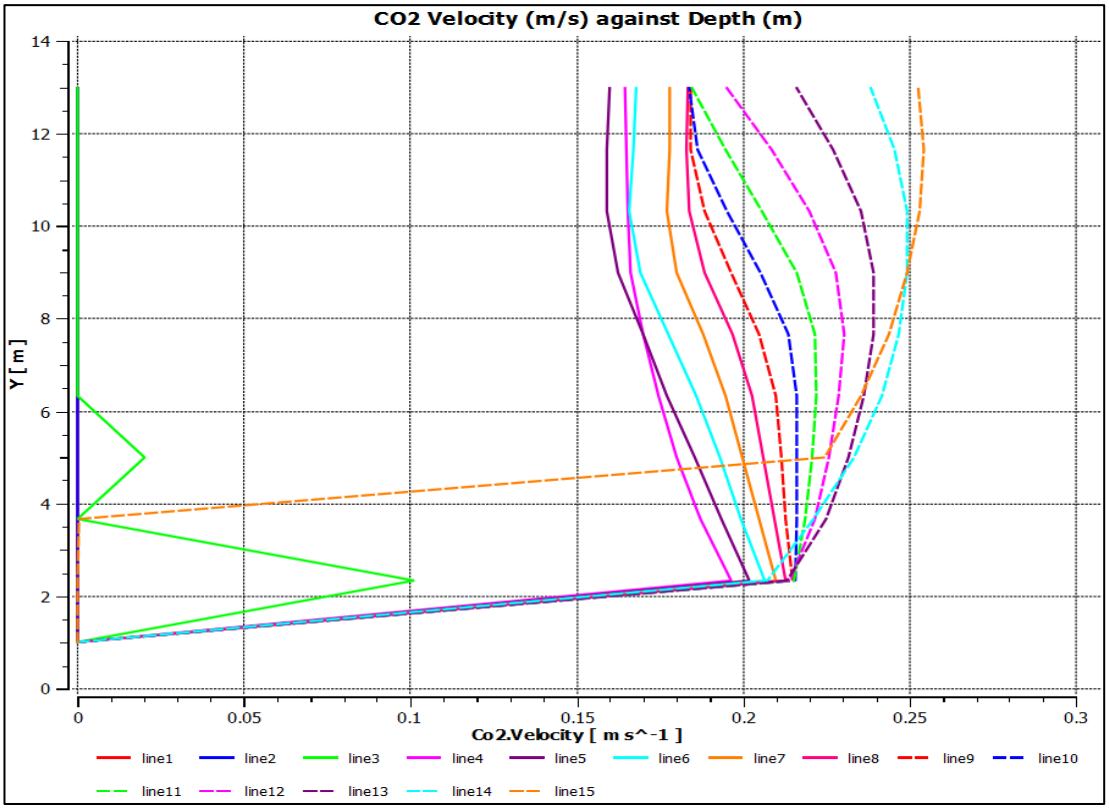


FIGURE 4.12 $CO_2$ velocity (m/s) against depth (m) for high tide release

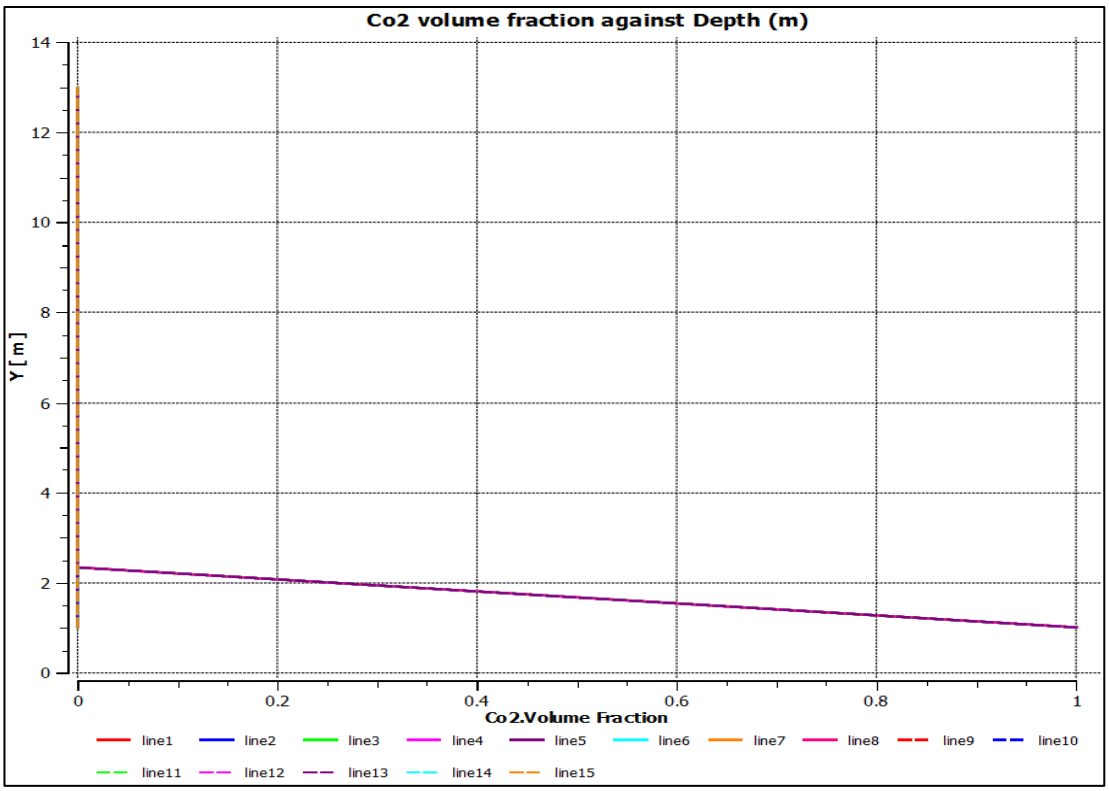


FIGURE 4.13 $CO_2$ volume fraction against depth (m) for high tide release

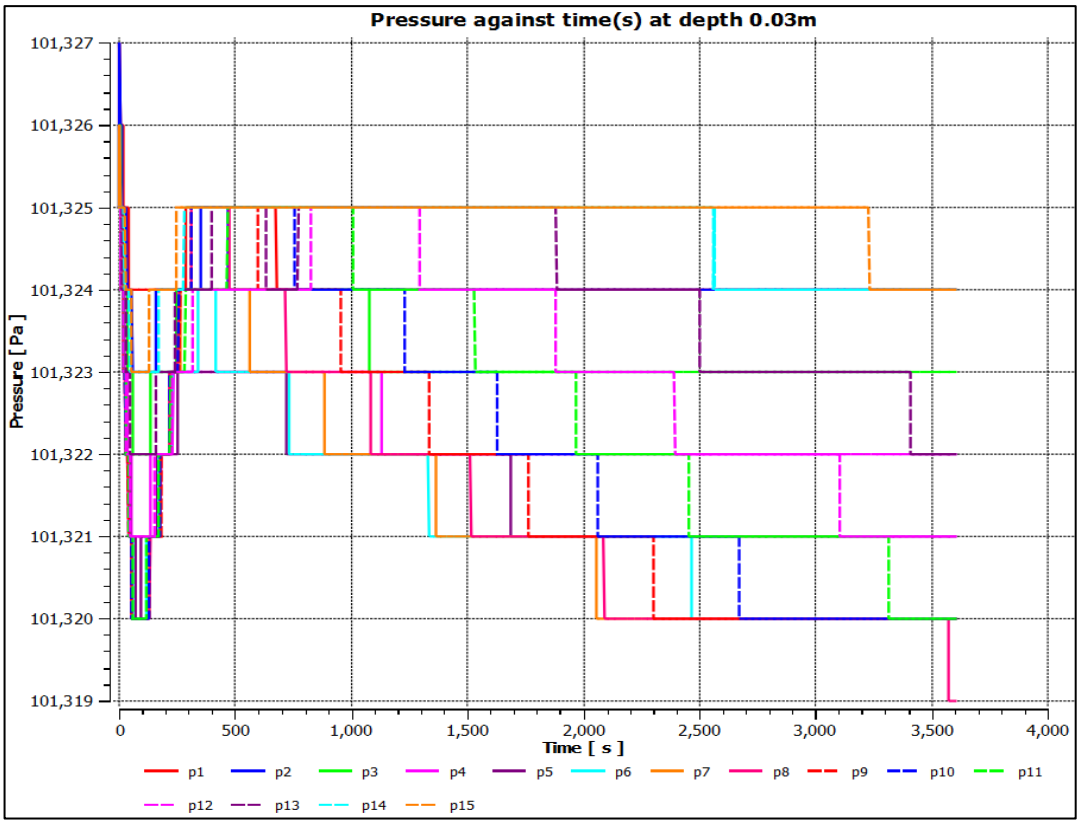


FIGURE 4.14 Pressure measured at depth 3cm for high tide release

APPENDIX 3

TABLE 4.3 $k_1$, $k_2$ and $k_w$ value for low tide release

| Sample | Pressure (Mpa) | $k_1$ | $k_2$ | $k_w$(0.1 Mpa) | $k_w$ |
|---|---|---|---|---|---|
| 1 | 0.101324 | 63.73820192 | 103.4293472 | 3.4955409E-15 | 3.5009080790E-15 |
| 2 | 0.101324 | 63.73820192 | 103.4293472 | 3.4955409E-15 | 3.5009080790E-15 |
| 3 | 0.101323 | 63.73883098 | 103.4303679 | 3.4955409E-15 | 3.5009080473E-15 |
| 4 | 0.101322 | 63.73946005 | 103.4313888 | 3.4955409E-15 | 3.5009080156E-15 |
| 5 | 0.101322 | 63.73946005 | 103.4313888 | 3.4955409E-15 | 3.5009080156E-15 |
| 6 | 0.101321 | 63.74008914 | 103.4324096 | 3.4955409E-15 | 3.5009079839E-15 |
| 7 | 0.10132 | 63.74071824 | 103.4334304 | 3.4955409E-15 | 3.5009079522E-15 |
| 8 | 0.10132 | 63.74071824 | 103.4334304 | 3.4955409E-15 | 3.5009079522E-15 |
| 9 | 0.10132 | 63.74071824 | 103.4334304 | 3.4955409E-15 | 3.5009079522E-15 |
| 10 | 0.10132 | 63.74071824 | 103.4334304 | 3.4955409E-15 | 3.5009079522E-15 |
| 11 | 0.10132 | 63.74071824 | 103.4334304 | 3.4955409E-15 | 3.5009079522E-15 |
| 12 | 0.101321 | 63.74008914 | 103.4324096 | 3.4955409E-15 | 3.5009079839E-15 |
| 13 | 0.101322 | 63.73946005 | 103.4313888 | 3.4955409E-15 | 3.5009080156E-15 |
| 14 | 0.101324 | 63.73820192 | 103.4293472 | 3.4955409E-15 | 3.5009080790E-15 |
| 15 | 0.101324 | 63.73820192 | 103.4293472 | 3.4955409E-15 | 3.5009080790E-15 |

TABLE 4.4 $k_1$, $k_2$ and $k_w$ value for high tide release

| Sample | Pressure (Mpa) | $k_1$ | $k_2$ | $k_w$(0.1 Mpa) | $k_w$ |
|---|---|---|---|---|---|
| 1 | 0.101324 | 63.73820192 | 103.4293472 | 3.4955409E-15 | 3.5009080790E-15 |
| 2 | 0.101324 | 63.73820192 | 103.4293472 | 3.4955409E-15 | 3.5009080790E-15 |
| 3 | 0.101323 | 63.73883098 | 103.4303679 | 3.4955409E-15 | 3.5009080473E-15 |
| 4 | 0.101322 | 63.73946005 | 103.4313888 | 3.4955409E-15 | 3.5009080156E-15 |
| 5 | 0.101321 | 63.74008914 | 103.4324096 | 3.4955409E-15 | 3.5009079839E-15 |
| 6 | 0.10132 | 63.74071824 | 103.4334304 | 3.4955409E-15 | 3.5009079522E-15 |
| 7 | 0.101319 | 63.74134734 | 103.4344513 | 3.4955409E-15 | 3.5009079205E-15 |
| 8 | 0.101319 | 63.74134734 | 103.4344513 | 3.4955409E-15 | 3.5009079205E-15 |
| 9 | 0.101319 | 63.74134734 | 103.4344513 | 3.4955409E-15 | 3.5009079205E-15 |
| 10 | 0.10132 | 63.74071824 | 103.4334304 | 3.4955409E-15 | 3.5009079522E-15 |
| 11 | 0.10132 | 63.74071824 | 103.4334304 | 3.4955409E-15 | 3.5009079522E-15 |
| 12 | 0.101321 | 63.74008914 | 103.4324096 | 3.4955409E-15 | 3.5009079839E-15 |
| 13 | 0.101322 | 63.73946005 | 103.4313888 | 3.4955409E-15 | 3.5009080156E-15 |
| 14 | 0.101324 | 63.73820192 | 103.4293472 | 3.4955409E-15 | 3.5009080790E-15 |
| 15 | 0.101324 | 63.73820192 | 103.4293472 | 3.4955409E-15 | 3.5009080790E-15 |